RSC Advances

ROYAL SOCIETY OF CHEMISTRY

www.rsc.org/advances

Role of Zinc and Copper metal ions in Amyloid β-peptides $A\beta_{1-40}$ and $A\beta_{1-42}$ Aggregation

Subramaniam Boopathi,[a] and Ponmalai Kolandaivel*[a]

Department of Physics, Bharathiar University, Coimbatore-46

Corresponding author mail: Ponkvel@hotmail.com

Fax No: +91-422-2422387

ABSTRACT

The aggregation of Amyloid β-peptides (Aβ) plays a key role in the central pathological pathways in Alzheimer's disease. The interaction of zinc and copper metal ions with Aβ-peptide gives considerable understanding to fight this incurable disease. The different conformations of native and metal interacted Aβ-peptides were investigated using molecular dynamics simulations for 50ns. $A\beta_{1-40}$-Zn^{2+} peptide adopts β-hairpin structure, which was promoted by turn region (Val24-Asp27) and increases the hydrophobic contact between the central hydrophobic (CHC) (Leu17-Ala21) and c-terminal (Met35-Val40). The turn region was stabilized by forming salt-bridge between Asp23-Lys28 and Glu22-Lys28 residues. The structure of $A\beta_{1-42}$-Zn^{2+} peptide was destabilized by the β-hairpin structure due to the absence of salt-bridge, and reduces the hydrophobic contact between CHC and c-terminal, which results in $A\beta_{1-42}$ monomers disaggregation. $A\beta_{1-40}$-Cu^{2+} peptide has three bend regions, which are separated by coil segment. These segments reduce the hydrophobic contact between CHC and c-terminal, and promote the formation of salt-bridge which in turn destabilizes the turn region of the peptide. The hairpin conformation of $A\beta_{1-42}$-Cu^{2+} structure was stabilized by increasing the hydrophobic contact and salt-bridge which is facilitated for aggregation.

Keywords: Aβ-peptides, Alzheimer's disease, molecular dynamics simulations, salt-bridge, disaggregation.

1. INTRODUCTION

Aggregation of Amyloid β-peptide (Aβ) is considered as a hallmark for the progression of Alzheimer's disease (AD) which is a debilitating neurodegenerative disorder. It affects about 5.4 million Americans and 25 million people worldwide, and these numbers are expected to increase dramatically.[1] Epidemiological studies have found that the incident of AD among people in their 70s was about 4 to 5 times lesser in India than in US. [2,3] The patient with AD, lose memory, slow in communication, and experience problems with visual-spatial search, along with other side effects. [4-6] Amyloid β-peptide (Aβ) is derived from the proteolytic cleavage of amyloid precursor protein (APP) by β- and γ-secretase enzymes. Aβ-peptide contains 40, and 42 amino acid residues whose progression appeared from a unstructured monomer to hairpin structure. The fibrillar aggregate associated with onset to Alzheimer's disease.[4,5] Recent investigations have reported that besides the Amyloid plaques with characteristic cross β-pattern structure, neurotoxicity can be induced by formation of oligomers of the Aβ-peptides. [7-10] In AD brains, accumulation of misfolded Aβ peptides and ptau proteins were observed.[1] It is still not clear, how these misfolded aggregates are involved in the onset and progression of disease. Kodali et al reported that the five $A\beta_{1-40}$ peptide structures have formed the fibril with β-sheet.[11] Solid state NMR measurement on $A\beta_{1-40}$ and $A\beta_{1-42}$ amyloid fibrils reveals the arrangement of parallel β-sheet within the protofilaments.[8] The major difference between the $A\beta_{1-40}$ and $A\beta_{1-42}$ peptides is the absence or presence of c-terminal dipeptides (e.g. two hydrophobic residues Ile41-Ala42). The Aβ peptides have the following primary structure:

$DAEFR_5HDSGY_{10}EVHHQ_{15}KLVFF_{20}AEDVG_{25}SNKGA_{30}IIGLM_{35}VGGVV_{40}IA_{42}$

The previous studies suggest that three distinct regions of the Aβ monomer, the central hydrophobic core (Leu17-Ala21), a turn region (Val24-Asp27), and second

hydrophobic region (Gly29-Met35) play an important role in aggregation process.[9-15] Fluoresence resonance energy transfer study indicates that $A\beta_{1-40}$ forms the stable monomer, dimmer, trimmer and tetramer, where as $A\beta_{1-42}$ forms the stable pentamer, hexamer and other larger assemblies.[16,17] Cryo-electron microscopy studies have shown that the complex polymorphism of Aβ fibrils characterised by size, cross section and width.[18,19] The salt bridge between Asp23 and Lys28 stabilizes the β-turn and, therefore, the entire β-hairpin structure promotes the nucleation for fibril growth.[20] Experimental and computational studies have addressed the mechanism of folding and oligomerization for $A\beta_{1-40}$ and $A\beta_{1-42}$ peptides.[7-10,21-28] Even though these studies offer precise information on the average structure, the atomic level knowledge on $A\beta_{1-40}$ and $A\beta_{1-42}$ monomers are essential to understand the aggregation process since they are the building blocks for larger oligomers. Normally, Aβ-peptide exists as a α-helix along with some random coil structure, but can be misfold into a β-sheet, which aggregates into amyloid oligomers leading to insoluble amyloid fibrils. The mechanism of this misfolding of Aβ peptide has not yet been understood properly. Many research groups have put their efforts to study the interaction of metal ions with monomeric Aβ peptide, and they try to correlate this with amyloid plaque formation.[29-36]

The structure of Aβ–Zn^{2+},[37,38] and Aβ–Cu^{2+} have been investigated in detail by NMR,[30-33] X-ray absorption spectroscopy,[34,35] and Fourier transform infrared spectroscopy.[36] Solid state NMR results help to identify the Zn^{2+} binding sites to characterise the critical structural changes induced by Zn^{2+} binding to the pathologically relevant $A\beta_{1-42}$ aggregates.[31,33] Mithu et al have identified that the Zn^{2+} binding breaks the salt-bridge between Asp23 and Lys28 residues by driving these residues into non salt-bridge conformation, where the unperturbed cross β-structure of $A\beta_{1-42}$ aggregates and increased the toxicity.[33] Hane et al. [39] have concluded that Cu and Cu^{2+} ions play a significant role to increase the binding between the two single Aβ-peptides. Nair et al.[40] have found that copper

binds with His residue with greater affinity than zinc, which significantly stabilizes the Aβ aggregation. High resolution structural studies of amyloid peptide by NMR experiment confirm the zinc binding with His14, which induces the localized disruption of the secondary structure of amyloid peptide.[32] In AD, the concentration of Cu and Zn ions increased in plaques and reaches to 400μM and 1mM, respectively compared with the region outside the plaque.[41] The metal-Aβ interactions have been used to test therapeutic agents, and these efforts have been made to understand the molecular details of Cu^{2+} and Zn^{2+} binding with Aβ.[42,43] However, the role of metal ions in Aβ-peptide aggregation process still remains elusive. Detailed structural information would be highly valuable for revealing still unknown mechanisms of the Aβ aggregation.

Molecular dynamics (MD) simulation is a powerful tool to investigate the secondary structure of Aβ-peptides. Even though, the number of studies have been performed to investigate the structural insight of Aβ-peptides aggregation in the presence of metal ions, the process of aggregation of monomeric form of Aβ-peptide is not well understood. So, the main aim of the present study is to investigate the aggregation process of Aβ-peptide in the presence of metal ions by considering three different secondary structure regions 1. central hydrophobic core region (Leu17-Ala21), 2. loop region (Asp23-Lys28), 3. second hydrophobic region (Gly29-Met35) which are playing a major role for the aggregation. The hydrophobic interaction between the central hydrophobic core region and c-terminal, the formation of salt-bridge between Asp23(Glu22) and Lys28 residues play a critical role for the aggregation process. The metal interactions induce the significant changes in the hydrophobic interaction and salt-bridge. Further the change of hydrophobic, and hydrophilic characters of the residues promote the bend structure in Aβ peptide due to the interaction with water molecules. The dynamics of the hydrophobic interaction and salt-bridge of the Aβ peptide have been maped by the classical molecular dynamics simulation in the presence of metal

ions. The experimental observation of these informations are very difficult and sometimes impossible. So the present study helps to understand much better way the aggregation process of Aβ-peptide, which is missing in the literature.

2. COMPUTATIONAL PROCEDURE

2.1 Molecular Dynamics Simulation

The initial structures of $A\beta_{1-40}$ and $A\beta_{1-42}$ monomers were taken from NMR study (Pdb ID: 1BA4,[44] and 1IYT[45]). Metals (Cu^{2+}, Zn^{2+}) were allowed to interact with N-terminal of their monomers ($A\beta_{1-40}$-Cu^{2+}, $A\beta_{1-40}$- Zn^{2+}, $A\beta_{1-42}$- Cu^{2+} and $A\beta_{1-42}$- Zn^{2+}) . These monomers and their metal interacted complex were solvated in a water box separately. The solvent molecules were used with TIP3P water model.[46,47] Each solvated structures were optimized by the molecular dynamics (MD) simulation package GROMACS 4.5.6 version utilizing the OPLSAA force field.[48,49] Each structure was placed in the center of a box using three dimensional(3D) periodic boundary condition. Steepest descent minimization was performed for 500 steps prior to and after MD refinement. Equilibration was performed into two phases. In the first phase, a NVT ensemble applied for 50ps using Barendsen weak coupling to quickly heated to 300K.[50] In the second phase, a NPT ensemble employed for 50ps to maintain the constant temperature (300K) and pressure (1atm), where all atoms were allowed to move. The MD simulation was carried out under NPT ensemble condition and it ran for 50ns and the structures were saved at each picosecond for analysis. The long range electrostatic interactions were calculated by particle mesh Ewald method.[51] All the bond lengths were constrained using the leapfrog algorithm, allowing an integration time step of 2fs. A non bonded cut off 1.0nm was employed in the simulation and updated every 10fs and all the short range non bonded interaction cut off at 1.4nm.[52] PyMol and Chimera were used to visualize the molecular structure and additional analyses were assisted by origin60, GNU image manipulation program.[53,54] The trajectory files were analyzed through g_rmsd tool in

GROMACS utilities to obtain root mean square deviation (RMSD). The secondary structure analyses were performed employing the secondary structures of protein (DSSP) protocol, which interfaces with GROMACS through do_dssp tool.[55] To analyze the hydrogen bonds, a cutoff distance 0.35nm has been fixed. The solvent accessible surface area (SASA) per residue was calculated to identify the hydrophobic and hydrophilic nature of each residue of monomers. The contact maps used for a pair of amino acid side chain considered to be formed when a minimal distance between any pair of their atoms is less than 1.5nm. Independent simulation has been performed with different initial conformation for the Aβ-peptides in the presence of metal ions to verify the convergence of trajectories (Fig. S7).

3. RESULTS AND DISCUSSION

Full length of $A\beta_{1-40}$ and $A\beta_{1-42}$ monomers and their complex structures ($A\beta_{1-40}$-Cu^{2+}, $A\beta_{1-40}$-Zn^{2+} and $A\beta_{1-42}$-Cu^{2+}, $A\beta_{1-42}$-Zn^{2+}) have been considered to explore the conformational dynamics of these peptides in aqueous solution for 50ns MD simulation. The previous studies suggest that the simulation time should be sufficient to elucidate structural features of these peptides.[56-59] The loop region Asp23-Lys28, the central hydrophobic core Leu17-Ala21 and second hydrophobic domain Gly29-Met35 of Aβ peptide are playing critical role in aggregation mechanisms. [9-15,26] Which is the main thrust of the present study.

Molecular dynamics simulations pay the way for the indepth analysis of the structural changes upon metal ion interactions with N-terminal of Aβ –peptides. The deviation between Aβ monomer and their complex structures were evaluated by root mean square deviation (RMSD) values, which have calculated for six trajectories of $A\beta_{1-40}$, $A\beta_{1-40}$-Cu^{2+}, $A\beta_{1-40}$-Zn^{2+}, $A\beta_{1-42}$, $A\beta_{1-42}$-Cu^{2+} and $A\beta_{1-42}$-Zn^{2+} as a function of time (Fig. 1). For all the six structures, considerable structural changes have been observed during the initial 500ps lead to a RMSD 0.4-0.75nm.When it reaches a stable value around 0.9-1.1nm in $A\beta_{1-40}$, the value of the

trajectory decreases to 0.75-0.85nm during the interaction of Cu^{2+}. The $A\beta_{1-40}$-Zn^{2+} structure attained the stable value around 0.85-1.0nm during the simulation (0.5-50ns). The final RMSD values have been observed around 0.9-1.2nm for three structures i.e $A\beta_{1-42}$, $A\beta_{1-42}$-Cu^{2+} and $A\beta_{1-42}$-Zn^{2+}. The above RMSD values help to understand the deviation of the minimum energy structure from the native state due to the interaction of metal ions ($A\beta_{1-40}$-Cu^{2+}, $A\beta_{1-42}$-Zn^{2+}).

3.1 $A\beta_{1-40}$ monomer conformational dynamics in aqueous solution

The helical structure of $A\beta_{1-40}$,[44] and its conformational changes have been monitored in aqueous solution using chimera visual software for every 10ns (Fig.2). The contact map (Fig.8a) represents the interaction of His6-Gly9, Asp7-Gly9, Ala2-Arg5 and Tyr10-Gln15 residues. During the course of simulation, the Val12-Leu17 residues adopt alpha helical structure, His6 and Gly9 residues lead to the bend region (Fig.8a), which promotes the first 12 residues adopt hairpin structure, tail region extended with Asp1-Arg5 and Tyr10-Val12 residues. The above interactions help to stabilize the β-hairpin structure in the region Asp1-Gln15 residues.

Another twenty residues (Lys16-Met35) have been architectured by three important regions, the central hydrophobic core region (Leu17-Ala21), the loop region (Asp23-Lys28) and second hydrophobic region (Gly29-Met35). The central hydrophobic core (Leu17-Ala21) was completely transformed into β-bend structure during the 20-50 nanosecond simulation. We have performed a time dependent analysis for the salt-bridge to probe its effect on the stability of Aβ-peptide (Fig.S1a). The salt-bridge distance was calculated as the average distance between the CO_2(-) moiety of Asp23 (or Glu22) and the NH_3^+ in Lys28 residue in the Aβ peptide. The direct-salt-bridge appeared around 4.3Å, whereas indirect or water mediated salt-bridge was appeared between 4.3 and 7.0Å.[56] We observed the higher distance between

Asp23 and Lys28 residues which do not has a direct salt-bridge but the indirect salt-bridge was formed during the first twenty nanosecond simulation. Consequently, the direct salt-bridge was appeared between Glu22 and Lys28 residues during the 20-50 nanosecond simulation. The salt-bridge of Glu22-Lys28 residues is stronger than the indirect salt-bridge Asp23-Lys28 residues. This is due to the longer intra distance (4.3-8.5 Å) between the carboxyl group of Asp23 and amine group of Lys28 compared with solid state NMR model in which the distance is much shorter.[20] These results are in contrast to the previous MD simulation, where the probability of forming an intra molecular salt-bridge between Asp23 and Lys28 (42%) is higher than that of the salt-bridge between Glu22 and Lys28 (36%).[14] These interactions in the region Glu22-Lys28 maintains turn structure throughout the simulation.

The interaction between the hydrophobic part of the Lys28 side chain and Val24 residue stabilizes turn conformation, which occurs at a distance of 4.5 and 7.5 Å between Val24 and Asn27 residue. This conformation allows the interaction between the central hydrophobic core (Leu17-Ala21) and hydrophobic c-terminal. Consequently, the distance (Val24)-(Asn27) increases to 7.5-10.0 Å during 10-50 nanosecond simulation and the hydrophobic contact between the c-terminal and Leu17-Ala21 fragment is reduced (Fig.S3a). The force between the electrostatic Asp23-Lys28 and hydrophobic Val24-Lys28 stabilize the turn region Val24-Asn27. The stable turn in the Val24-Asn27 domain favours hydrophobic contact between the hydrophobic core (Leu17-Ala21) and the c-terminal. These results agree with the Lazo et al,[60,61] who have studied the hydrophobic contact within the decapeptide $A\beta_{21-30}$ using NMR study and MD simulation. The turn region plays a significant role in facilitating the formation of the bend in the Aβ peptide, which has been started from fifth nanosecond to the end of the simulation period. After 12ns, the Phe19-Asp23 region and second hydrophobic region (Gly29-Met35) were converted into the turn and beta bridge

197 structures (Fig.2a). The bend region (Val24-Asn27) is necessary to facilitate the parallel
198 architecture for long Aβ peptide, which agrees with the results of Tycko et al[8,22] who have
199 measured NMR spectra for $A\beta_{1-40}$. They have shown that the first β-sheet appeared after tenth
200 residue. The contact map shows the significant interaction between the Phe4-Leu34, Phe4-
201 Gly9, Gln15-Val18 and Ile31-Met35 residues. During the course of the simulation, the c-
202 terminal (Met35-Val40) residues have been changed between coil and bend, and turn
203 conformations. Our simulation result reveals that $A\beta_{1-40}$ is composed of coil components
204 (34%), helical content (18%), turn and bend conformation (43%) and β-structure (4%) in
205 aqueous solution (Table 1).

206 3.2 Interaction of Cu^{2+} with $A\beta_{1-40}$ monomer in aqueous solution

207 In human blood plasma, more than 98% of the amino acid bound with Cu^{2+} ion, which
208 occurs in histidine complex.[62] Cu^{2+} ion has higher affinity with three histidine residues of
209 $A\beta_{1-40}$ monomer.[38] The conformational changes of $A\beta_{1-40}$-Cu^{2+} structure have been monitored
210 in the explicit water. The conformational structures for every 10ns are displayed in Fig.3.
211 During the course of simulation, a significant difference has been noticed in $A\beta_{1-40}$-Cu^{2+}
212 structure. The NH of Glu3 residue and C=O group of backbone form the β-sheet hydrogen
213 bond with C=O and NH groups of His6 residue and its distance changed from 0.2 to 0.25nm.
214 This interaction helps for the formation of first bend structure which appears in the Glu3-His6
215 region. The strong interaction has been observed between Ala2 -His6 and Asp1-Asp7
216 residues, where the distances are varying between 0.15 and 0.25nm (Fig.8b). These
217 interactions have played a significant role to stabilize the bend structure (Glu3-His6) which
218 are helping to form a β-hairpin structure in the Asp1-Asp7 region.

219 The turn structure appears in the Asp23-Asp27 region (Fig.3a), was stabilized by the
220 strong hydrogen bond (0.2-0.3nm) between Glu22 and Ser26 residues. The turn structure has

attributed to the second bend structure in the Glu22-Lys28 region of $A\beta_{1-40}$- Cu^{2+} structure. The region (Val18-Lys28) exhibits helical conformation in the first 2ns, but after that, it completely transformed into turn structure during 2-45ns simulation. The helical structure exhibited in the Val18-Gly25 region of the $A\beta_{1-40}$ –Zn^{2+} structure. The (Val24)-(Asn27) distance has been changed between 0.55 and 0.75nm, and this interaction allows to increase the hydrophobic contact between the central hydrophobic core (Leu17-Ala21) and the c-terminal (Met35-Val40) region (Fig.S3a). The salt-bridge distance calculated between Asp23 and Lys28 residues is around 0.2-0.8nm during the first 10ns simulation. The salt-bridge disappeared after 10ns simulation, but the indirect salt-bridge has been formed between Glu22 and Lys28 residues. The absence of salt-bridge between Asp23 and Lys28 residues destabilize the turn structure, and contributed to depromote the β-hairpin conformation of $A\beta_{1-40}$-Cu^{2+} structure, which agrees with previous MD simulation of $A\beta_{1-40}$-Met35(O) monomer.[60]

The third bend region appears in the second hydrophobic region (Gly29-Met35). Gly29-Ile32 region undergoes a conformational change between turn and bend structures, which was stabilized by the interaction between C=O group of Ile32 and NH group of Lys28 residues and the distance is around 0.3-0.35nm. Subsequently, the c-terminal region (Met35-Val40) exhibits the coil structure throughout the simulation. The calculated SASA values (Fig.S4) reflect the increase in the hydrophobic character of Phe4 , Leu34 and Met35 residues in $A\beta_{1-40}$-Cu^{2+} structure as compared with $A\beta_{1-40}$-Zn^{2+} and $A\beta_{1-40}$ structures. The differences in the SASA values between $A\beta_{1-40}$-Cu^{2+} and $A\beta_{1-40}$ structures (Fig.S5), the positive and negative values represent the increase and decrease in the hydrophobic character. The difference in SASA value per residue indicate the increase of the hydrophobicity of Phe4, Leu34 and Met35 residues and increase the hydrophilic character of His6, Asp23 , Lys28 and Ile32 residues. Among these, His6 residue is more exposed to the interaction with water

which may be the reason to form first bend structure in the N-terminal of monomeric structure. The influence of hydrophobic/hydrophilic character on loop and SHC region, promote the bend structure during the interaction of $A\beta_{1-40}$-Cu^{2+} in aqueous solution. However, due to the hydrogen bonds between the side chains of Asp23 and Lys28 residues, and the surrounding water molecules, the salt-bridge between Asp23-Lys28 residues get disrupted. In comparison with $A\beta_{1-40}$-Zn^{2+} , the $A\beta_{1-40}$-Cu^{2+} structure possesses 11% less helical conformation, 7% less coil conformation , 5% less bend conformation, 4% more beta structure and 19% more turn conformation (Table 1). This shows that the helical structures were reduced, turn structure was destabilized and hydrophobic contact was reduced between SHC and C-terminal region of $A\beta_{1-40}$-Cu^{2+} structure.

3.3 Interaction of Zn^{2+} with $A\beta_{1-40}$ monomer in aqueous solution

Tycko et al. [33] have found that more than 90% of total Zn^{2+} was bound to Aβ aggregates. We have made molecular dynamics simulation for $A\beta_{1-40}$- Zn^{2+} structure in explicit water. This monomer exhibits two coil connected by the helical structure (Fig.4b). The first eleven residues adopt β-hairpin structure with β-bend in the Phe4-Lys6 residues, the tail structure extended with Asp1-Phe4 and Asp7-Glu11 residues, during the 24-50ns (Fig.4a). The alpha helical structure of Val12-Gln15 residues did not changed during the interaction of Zn^{2+} ion. The central hydrophobic residues (Leu17-Ala21) were transformed to alpha helical structure due to the strong electrostatic interaction between the i and i+3 residues which is represented in the contact map (Fig.8c).

The intra-chain salt bridge was observed between Glu22 and Lys28 residue, which persists throughout the simulation (5-40ns). The indirect salt bridge appeared between Asp23 and Lys28 residues (Fig.S1a) during the first 40ns simulation and subsequently direct salt-bridge was observed for the remaining simulation. The hydrophobic contact increases

between the hydrophobic residues (Leu17-Ala21) and c-terminal in the first 5ns and the remaining simulation period, the hydrophobic contact decreased due the increase in distance 0.7-1.0nm between C_α (Val24) and C_α(Asn27) residues (Fig.S3a).

In $A\beta_{1-40}$, the central hydrophobic core region (Leu17-Ala21) undergoes a conformational change between helix and turn structures which exhibits stable helix in $A\beta_{1-40}$-Zn^{2+} structure. In the second hydrophobic region (Gly29-Met35), the residues Gly33-Met35 form turn structure throughout simulation in $A\beta_{1-40}$, the same structure transformed from helix to coil in $A\beta_{1-40}$-Zn^{2+}. The above results show, the formation β-hairpin like structure is less probable during the Zn^{2+} ion interaction with $A\beta_{1-40}$monomer. The solvent accessible surface area (SASA) analyzed to find the hydrophobic character of individual residue of $A\beta_{1-40}$ monomer. The difference in SASA values per residue between the $A\beta_{1-40}$ – Zn^{2+} and reduced $A\beta_{1-40}$ structures is shown in Fig.S6, where the positive and negative values indicate the increase and decrease in hydrophobic character. The differences in the SASA values per residue indicate the enhancement of the hydrophobicity of Gln15, Val18, Ile32 and Met35 residues and subsequently increase the hydrophilic character of Lys16, Phe20, Asp23 and Lys28 residues.

When compare with $A\beta_{1-40}$ structure, the $A\beta_{1-40}$-Zn^{2+} structure has 10% more helical and 6% less turn and bend structures and 3% less β-sheet structures (Table 1). The distance calculated between CO_2^-(Asp23) and NH_3^+(Lys28) is greater than 0.8nm during 5-40ns simulation. During the same period, the distance between CO_2^-(Glu22) and NH_3^+(Lys28) residues has been observed around 0.22-0.45nm.This is due to the presence of salt-bridge. The Glu22-Lys28 region promotes stronger stabilization in the turn structure, when compared with Asp23-Lys28 region of $A\beta_{1-40}$–Cu^{2+} structure. The hairpin like structure was stabilized by stronger salt-bridge formation between Glu22-Lys28 and Asp23-Lys28 residues during the Zn^{2+} ion interaction and it allows to form the greater rate of aggregation compared with

Cu^{2+} ion interaction with N-region of $A\beta_{1-40}$ monomer. This result agrees Noy et al NMR study that Zn^{2+} interaction with Aβ, causes rapid aggregation into nonfibrillar species.[63]

3.4 $A\beta_{1-42}$ monomer conformational dynamics in aqueous solution:

The $A\beta_{1-40}$ and $A\beta_{1-42}$ are the most abundant in nuetritic amyloid plaques, the presence of two hydrophobic residues, Ile41 and Ala42 at the c-terminal leads to distinct oligomeric distribution during fibrilization in invitro. We investigated the structural differences between $A\beta_{1-40}$ and $A\beta_{1-42}$ monomers (Table 1), where the $A\beta_{1-42}$ possesses 28% more helical, 9% less coil, 7% less bend and 7% less turn structure than the $A\beta_{1-40}$. The distance calculated between Asp23 and Lys28 residues is greater than 0.9nm, which indicate the absence of salt-bridge throughout the simulation period of $A\beta_{1-42}$ monomer, whereas $A\beta_{1-40}$ monomer has direct salt bridge (<0.43nm) during the last 30ns simulation. However the salt-bridge was observed between Glu22 and Lys28 residues of $A\beta_{1-42}$ monomer (Fig.S2b), where the interaction distance changes between 0.2 and 0.7nm during 22-50ns simulation. The turn structure (Val24-Asn27) was stabilized by salt-bridge of Glu22-Lys28 residues of both monomers, but the shape of the β-hairpin like structure in the $A\beta_{1-42}$ monomer located in the middle region (Asp23-Asn27) has a larger curvature than that observed in $A\beta_{1-40}$ monomer.

Fig.S3b shows, the distance between C_α(Val24) and C_α(Asn27) residues is around 0.4-0.65nm, which increases the hydrophobic interaction between the central hydrophobic region (Leu17-Ala21) and c-terminal region during the first 10ns. The $A\beta_{1-42}$ monomer was formed by stronger hydrophobic interaction between the central hydrophobic region and c-terminal. Among the first ten residues (Asp1-Tyr10), Glu3-His6 residues form helical structure during the first 27ns simulation and during further simulation (27-40ns), it fluctuates between turn and helical conformations. In contrast to the $A\beta_{1-40}$ monomer, the

region (Asp1-Tyr10) adopts bend structure during the simulation period. The 28% more helical structure was observed in the first twenty three residues (Asp1-Asp23) because of the presence of hydrophobic dipeptide in the c-terminal region.

The differences in the SASA values of $A\beta_{1-40}$ and $A\beta_{1-42}$ monomers (Fig.9a), indicate the presence of (Ile41-Ala42) dipeptide, significantly enhances the hydrophobicity of Phe4, Gln15, Phe19 residues and subsequently increases the hydrophilic character of His13, Leu17, Val40 residues. These results indicate that the hydrophobic and hydrophilic characters help to maintain the helical structure in the Try10-Asp23 residues of the $A\beta_{1-42}$ monomer in aqueous solution. The overall result suggested that the β hairpin like structure was stabilized by the salt-bridge between Glu22-Lys28 residues. This result agrees with the experimental result of $A\beta_{1-42}$ monomers, where it aggregates faster than $A\beta_{1-40}$ monomers.[16,17,22,29]

3.5 Interaction of Cu^{2+} with the $A\beta_{1-42}$ monomer in aqueous solution

The structural changes of $A\beta_{1-42}$ monomer induced by Cu^{2+} ion were studied by x-ray diffraction, NMR, absorption spectroscopy, Atomic force spectroscopy and Fourier transform infrared spectroscopy.[22,29,31,34-36,39] In the first ten residues of $A\beta_{1-42}$-Cu^{2+} structure, Asp1-Phe4 segment shows coil, Arg5-Tyr10 segments adopt turn and bend structures. The stronger interaction has been noticed between Phe4-Ser8 and Arg5-Tyr10 residues (Fig.8e), which transforms the alpha helix to turn and bend conformational structures, but this was completely missing in $A\beta_{1-40}$-Cu^{2+} structure. The Cu^{2+} ion change the alpha helix to the turn conformation in the His13-Asp23 region of $A\beta_{1-42}$ monomer after 30ns simulation period. The $A\beta_{1-42}$-Cu^{2+} structure has 10% more helical structure than the $A\beta_{1-40}$-Cu^{2+} in the first twenty four residues (Fig.6a and Table 1).

We found the stronger hydrogen bond between N-H group of Asn27 and C=O group of Gly37 residue in $A\beta_{1-42}$ –Cu^{2+} structure. The Gly33 residue has interacted with

Gly37 and Ser26 residues in $A\beta_{1-42}$-Cu^{2+} structure, whereas in the $A\beta_{1-40}$-Cu^{2+} structure, these interactions are completely missing (Fig.8e). The above interactions have attributed to the formation of β-hairpin like structure in the Lys28-Ala42 region. Some significant differences have been noticed in the loop region of Asp23-Lys28 residues during the interaction of Cu^{2+} ion in the $A\beta_{1-42}$ monomer. The salt-bridge formed between Glu22 and Lys28 residues of $A\beta_{1-42}$ monomer (Fig.S2b), converted into the indirect salt-bridge when Cu^{2+} ion interacted with monomer. However in the $A\beta_{1-40}$-Cu^{2+} structure, the indirect salt-bridge formed between the same residues.

The observed hydrophobic contact increased between central hydrophobic region (Leu17-Ala21) and N-terminal, when Cu^{2+} ion interacted with monomer, the same contact decreased due to the increasing distance around 0.45-0.65nm between C_α (Val24) -C_α(Asn27) residues during the first 25ns (Fig.S3b). In the $A\beta_{1-40}$-Cu^{2+} structure, the calculated distance between them is greater than 0.6nm, so the hydrophobic contact get reduced throughout the simulation. The hydrophobic contact between CHC and c-terminal is stronger in $A\beta_{1-42}$-Cu^{2+} compared with $A\beta_{1-40}$-Cu^{2+} structure. The differences in the SASA values per residue (Fig.9b) indicate that the presence of the hydrophobic dipeptides which significantly enhances the hydrophilic character of Arg5, His13 and increases the hydrophobic character of Asp1, Ala2 and Lys28 residues. If the Cu^{2+} ion interacts with His13, His14 and His6 residues, it promotes the stabilization in the β-hairpin structure. This was realized by the parallel sheet arrangement, in which Cu^{2+} coordinated with the N-terminal. Experimental results show that Cu^{2+} ions were bridged by two His13 (or His14) rings of each two single β-peptide.[39] Our results indicate that the hairpin like conformation was stabilized by the presence of salt-bridge between Asp23-Lys28, Glu22-Lys28 residues, and hydrophobic interaction between CHC and c-terminal.

3.6 Interaction of Zn^{2+} with the $A\beta_{1-42}$ monomer in aqueous solution

The first ten residues of $A\beta_{1-42}$-Zn^{2+} structure forms the 3_{10}-helical structure, the N-H group of Ala2 makes hydrogen bond with C=O group of Arg5 residue (Fig.8f).This interaction was absent in the $A\beta_{1-42}$-Cu^{2+} and $A\beta_{1-40}$-Zn^{2+} structures. The next five residues (His6-Tyr10) exhibit bend and turn conformations in $A\beta_{1-42}$-Zn^{2+} structure. Helix has been formed by the His13-Glu22, and Gly9-Glu22 residues of $A\beta_{1-40}$-Zn^{2+}. The differences in SASA value per residue between $A\beta_{1-42}$-Zn^{2+} and $A\beta_{1-40}$-Zn^{2+} structures (Fig.9c) increases the hydrophobicity of Phe19 residue and enhances the hydrophilic character of Glu11, His14 and Leu17 residues. The $A\beta_{1-42}$-Zn^{2+} structure possesses 8% more helical and 10% less coil structures than the $A\beta_{1-40}$-Zn^{2+} structure (Fig.7a).

The Zn^{2+} interaction has promotes the significant structural changes in the N-terminal loop region connecting the two hydrophobic domain. The major change was, the disappearance of the salt-bridge between Asp23 and Lys28 residues. The hydrophobic contact between central hydrophobic core and c-terminal decreases in the $A\beta_{1-42}$-Zn^{2+} structure than that of $A\beta_{1-42}$-Cu^{2+} and $A\beta_{1-40}$-Zn^{2+} structures. These results suggest that the rate of aggregation increases in the $A\beta_{1-42}$ monomer due to the interaction of Cu^{2+} than Zn^{2+}.

4. CONCLUSION

Molecular dynamics simulation has been performed to investigate the conformational and structural changes in $A\beta_{1-40}$ and $A\beta_{1-42}$ monomers with and without interaction of metal ions (Cu^{2+},Zn^{2+}) in explicit water for 50ns simulation. This simulation has elucidated the atomic level calculation for three important regions (central hydrophobic domain (Leu17-Ala21), loop region (Asp23-Lys28) and second hydrophobic region (Gly29-Met35)) of the monomers. The presence of hydrophobic dipeptide in $A\beta_{1-42}$ monomer, the significant structural changes have been observed in the secondary structure. For instance, the CHC (Leu17-Ala21) region contains Tyr10-Asp23 residues exhibits alpha helix, whereas in $A\beta_{1-40}$,

region adopts helix and bend conformations. The $A\beta_{1-42}$ monomer possesses 28% more helical structure between Asp1-Lys28 residues as compared with $A\beta_{1-40}$ monomer. However in the $A\beta_{1-42}$ monomer, the loop region (Asp23-Lys28) and salt-bridge disappeared, where as in $A\beta_{1-40}$ monomer salt-bridge often forms during the course of simulation. The hydrophobic contact between C-terminal and CHC region increases and a small curvature forms in the turn region(Val24-Asn27) in $A\beta_{1-42}$ monomer. In the second hydrophobic region, bend conformation has been observed in $A\beta_{1-42}$, whereas in the $A\beta_{1-40}$, this exists in turn and beta bridge regions. Aforementioned processes have stabilized the β-hairpin like structure in $A\beta_{1-42}$ monomer and it leads to provide the chance to attach the new β-hairpin monomer.

In the $A\beta_{1-42}$-Zn^{2+}structure, Asp1-Tyr10 residues form the 3_{10}-helix and coil conformation, but these are transformed to bend conformations in $A\beta_{1-40}$ monomer. The CHC(Leu17-Ala21) region contains Tyr10-Val24 residues of $A\beta_{1-42}$-Zn^{2+}which exists in the helical conformation throughout the simulation and this region transforms into bend (Tyr10-His13) and helical (His13-Val24) conformations in $A\beta_{1-40}$-Zn^{2+} structure. Surprisingly in the $A\beta_{1-42}$-Zn^{2+} structure, salt-bridge was disappeared in Asp23-Lys28 residues but it often forms in $A\beta_{1-40}$-Zn^{2+} structure throughout the simulation period. The turn (Val24-Asp27) region was stabilized due to the salt-bridge between Glu22-Lys28 residue in $A\beta_{1-42}$-Zn^{2+} structure and where as $A\beta_{1-40}$-Zn^{2+} structure was stabilized by salt-bridge between Asp23-Lys28 and Glu22-Lys28 residues. The second hydrophobic region (Gly29-Met35) forms bend and coil conformations in $A\beta_{1-42}$-Zn^{2+}, whereas in $A\beta_{1-40}$-Zn^{2+} structure, this region exhibits the helix and bend conformations. The hydrophobic contact between c-terminal (Met35-Val40) and CHC was decreased in the $A\beta_{1-42}$-Zn^{2+} structure than in the $A\beta_{1-40}$-Zn^{2+}. This structural difference has prevent to attach the new incoming β-hairpin monomer when the interaction of Zn^{2+} with $A\beta_{1-42}$ monomer.

In $A\beta_{1-42}$-Cu^{2+} structure, the CHC (Leu17-Ala21) residues become alpha helical and turn conformers, whereas in $A\beta_{1-40}$-Cu^{2+} structure, this region adopts turn conformation. However the loop region (Asp23-Lys28) and turn region, Val24-Asn27 residues stabilized by salt-bridge formation between Asp23-Lys28 and Glu22-Lys28 residues in $A\beta_{1-42}$-Cu^{2+}as compared with the $A\beta_{1-40}$-Cu^{2+}. The $A\beta_{1-40}$-Cu^{2+} structure divided into three bend structures separated by coil segment. The interaction distance between C_α(Val24) and C_α(Asn27) residues is responsible for increasing the hydrophobic contact between CHC and c-terminal (Met35-Val40) in $A\beta_{1-42}$-Cu^{2+} structure. The second hydrophobic region has bend conformation in $A\beta_{1-42}$-Cu^{2+} structure, whereas in $A\beta_{1-40}$-Cu^{2+}, this region transforms to the turn and β-bridge conformations. This structural differences lead to stabilize the β-hairpin structure of $A\beta_{1-42}$-Cu^{2+} structure and it gives chance to form the fast fibrilization of Amyloid protein. Further, it has been found that the interaction of Cu^{2+} and Zn^{2+} with $A\beta_{1-40}$ and $A\beta_{1-42}$ is maximum at the beginning of the simulation, and fluctuates around 1-2nm during the simulation period.

SUPPORTING INFORMATION

The salt-bridge was formed between the CO_2^- moiety of Asp23 (or Glu22) and the NH_3^+ in Lys28 residue as a function of time, which is shown in Fig. S1-S2. Distance between Cα (Val24) and Cα (Asn27) as a function of time is shown in Fig. S3. Solvent accessible surface area analysis of the $A\beta_{1-40}$, $A\beta_{1-40}$-Cu^{2+} and $A\beta_{1-40}$-Zn^{2+} structures are shown in Fig. S4 – S6. Convergence of trajectories for different conformation are given in Fig. S7.

ACKNOWLEDGEMENT

The authors are thankful to DST (Department of Science and Technology) for the financial support in the form of project (SR/CSI/31/2011G dated 07-03-2012) under Cognitive Science Initiative (CSI) scheme.

REFERENCES

1 G. Ciprani, C. Dolciotti, L. Pichi and V. Bonucelli, *Neurol. Sci*. 2011, **32,** 260-279.

2 T. P. Ng, P. C. Chiam, T. Lee, H. C. Chau, L. Lim and E. H. Kau, *Am. J. Epidemiol.* 2006, **164**, 898-906.

3 R. Pandav, S. H. Bells and S. T. Dekosky, *Arch. Neurol.* 2005**, 60**, 824.

4 K. Blennow, M. J. De Leon and H. Zetterberg, *Lancet.* 2006, **368**, 387.

5 M. P. Mattson, *Nature* 2004, **430**, 631.

6 G. M. Mckhann, D. S. Knopman, H. Chertkow, B.T. Hyman, C. R. Jack, Jr, C. H. Kawas, W. E. Klunk, W. J. Koroshertz, J. J. Manly, R. Mayeux and R. Mohs, *Alzheimer's Disease* 2011, **7**, 268.

7 J. D. Pham, N. Chim, C. W. Gouldinng and J. S. Nowick, *J. Am. Chem. Soc.* 2013, **135**, 12460-12467.

8 R. Tycko and R. B. Wickner, *Accounts of Chemical Research.* 2013, **46**, 1487-1496.

9 W. M. Berhanu and U. H. E. Hansmann, *PLos ONE*. 2012**,7,** e41479.

10 A. T. Petkova, R. D. Leapman, Z. Guo, W. Yau, M. P. Mattson and R. Tycko, *Science*. 2005, **307**, 262-265.

11 R. Kodali, A. D. Williams, S. Chemura and R. Wetzel, *J. Mol. Biol.* 2010, **401**, 503-517.

12 U. Anand and M. Mukherjee, *Langmuir.* 2013, **29**, 2713-2721.

13 B. Tarus, J. E. Straub and D. Thirumalai*, J. Am. Chem. Soc.* 2006, **128**, 16162-16168.

14 A. Melquiond, X. Dong, N. Mousseau and P. Derreumaux, *Curr. Alzheimer. Res.* 2008, **5**, 244-250.

15 K. Ono, M. M. Condron and D. B. Teplow, *J. Biol. Chem*. 2010, **285**, 23186-23197.

16 W. Garzon-Rodriguez, A. Vega, M. Sepulveda-Becerra, S. Melton, D. A. Johnson, A.K. Yatsimirsky, et al. *J. Biol. Chem.* 2000, **275**, 22645-26649.

17 Y. R. Chen and C. G. Glave, *J. Biol. Chem.* 2006, **281**, 24414-24422.

18 C. Sachse, M. Fandrich and N. Grigorieff, *Proc. Natl. Acad. Sci. U.S.A.* 2008, **105**, 7462-7466.

19 M. Schmidt, C. Sachse, W. Richter, C. Xu, M. Fandrich, et al. *Proc. Natl. Acad. Sci. U.S.A.* 2009, **106**, 19813-19818.

20 A. T. Petkova, W. M. Yau and R. Tycko, *Biochemistry* 2006, **45**, 498-512.

21 D. B. Teplow, N. D. Lazo, G. Bitan, S. Bernstein, T. Wyttenbach, M. T. Bowers, A. Baunketner, J. Shea, B. Urbnc, L. Cruz, et al. *Acc. Chem. Res.* 2006, **39**, 635-645.

22 I. W. Hamley, *Chem. Rev.* 2012, **112**, 5147-5192.

23 C. Ritter, M. I. Maddelein, A. B. Siemer, T. Luhrs, M. Ernst, B. H. Meier, S. J. Saupe and R. Riek, *Nature* 2005, **435**, 844-848.

24 R. Nelson, M. R. Sawaya, M. Balbrinie, A. O. Madsen, C. Rickel, R. Grothe and D. Eisenberg, *Nature* 2005, **435**, 773-778.

25 B. Urbanc, L. Cruz, D. B. Teplow and H. E. Stanley, *Curr. Alzheimer. Res*. 2006, **3**, 493-504.

26 J. A. Lemkul and D. R. Bevan, *J. Phys. Chem. B.* 2010, **114,** 1652-1660.

27 S. Boopathi and P. Kolandaivel, *J. Mol. Model.* 2014, **20** (3), 2109.

28 T. Luhrs, C. Ritter, M. Adrian, D. Rick-Loher, B. Bohrmann, H. Dobeli, D. Schubert and R. Riek, *Proc. Natl. Acad. Sci. U.S.A.* 2005, **29**, 17342-17347.

29 K. P. Kepp, *Chem. Rev.* 2012, **112**, 5193-5239.

30 E. Gaggelli, A. Janicka-Klos, E. Jankowska, H. Kozlowski, C. Miglionni, E. Molteni, D. Valensin and E. Wieczerzak, *J. Phys. Chem. B.* 2008, **112**, 100.

31 S. Parthasarathy, F. Long, Y. Miller, Y. Xiao, D. Mc Elheny, K. Thurber, B. Ma, R. Nassinov and Y. Ishii, *J. Am. Chem. Soc.* 2011, **133**, 3390-3400.

32 J. R. Brender, K. Hartman, R. P. Reddy Nanga, V. Popovych, R. D. L. Salud Bea, S. Vivekanandhan, E. N. G. Marsh and A. Ramamoorthy, *J. Am. Chem. Soc.* 2010, **132**, 8973-8983.

33 V. S. Mithu, B. Sarkar, D. Bhowmik, M. Chandrakesan, S. Maiti and P. K. Madhu, *Biophysical Journal.* 2011, **101**, 2825-2832.

34 S. Morante, *Curr. Alzheimer. Res.* 2008, **5**, 508.

35 P. Faller and C. Hureau, *Actual. Chim.* 2011, **88**, 356-360.

36 Y. El Khoury, P. Dorlet, P. Faller and P. Hellwig, *J. Phys. Chem. B.* 2011, **115**, 14812.

37 A. K. Sharma, S. T. Pavlova, D. Finkelstein, N.J. Hawco, N. P. Rath, J. Kim and L. M. Mirica, *J. Am. Chem. Soc.* 2012, **134**, 6625-6636.

38 A. Asandei, I. Schiopu, S. Iftemi, L. Mereuta and T. Luchian, *Langmuir* 2013, **29,** 15634-15642.

39 F. Hane, G.Trans, S. J. Attwood and Z. Leonenko, *PLoS ONE.* 2013, **8**, e62005.

40 N. G. Nair, G. Perry, M. A. Smith and V. P. Reddy, *J. Alz. Dis.* 2010, **20**, 60-66.

41 M. Lovell, J. Robertson, W. Teesdale, J. Campbell and W. Markesbery, *J. Neurol. Sci.* 1998, **161**, 47-52.

42 A. I. Bush, *J. Alz. Dis.* 2008, **15**, 223-240.

43 J. S. Choi, J. J. Braymer, R. P. R. Nanga, A. Ramamoorthy and M. H. Lim, *Proc. Natl. Acad. Sci. U.S.A.* 2010, **107**, 21990-21995.

44 M. Coles, W. Bicknell, A. Watson, D. P. Fairliem and D. Craick, *J. Biochemistry.* 1998, **37**, 11064.

45 O. Crescenzi, S. Tomaselli, R. Guerrini, S. Salvatori, A. M. D'ursi, P. A. Temussi and D. Picone, *Eur. J. Biochem.* 2002, **269,** 5642-5648.

46 J. W. Jorgensen, J. Chandrasekhar, J. D. Madura, R. W. Imprey and M. L. Klein, *J. Chem. Phys.* 1983, **76**, 926.

513 47 S. Boopathi and P. Kolandaivel, *J. Biomol. Struct. Dyn.* 2013, **31**, 161-173.

514 48 B. Hess, C. Kutzner, D. Van der Spoel and E. Lindahl, *J. Chem. Theory. Comput.* 2008, **4,**

515 435-444.

516 49 G. A. Kaminski and R. A. Friesner, *J. Phys. Chem. B.* 2001, **105**, 6474-6487.

517 50 H. J. C. Berendsen, J. P. M. Postma, W. F. Van Gunsteren, A. Di Nola and J. R. Haak, *J.*

518 *Chem. Phys.* 1984, **81**, 3684-3690.

519 51 T. Darden and D. York, L. *J. Chem. Phys.* 1993, **98**, 10089-10092.

520 52 R. W. Hockney, S. P. Goel and J. Eastwood, *J. Comput. Phys.* 1974, **14**, 148-161.

521 53 W. L. De Lano, The PyMol Molecular graphics system. Version 1.1, LLC, 2008.

522 54 T. D. Goddard, C. C. Huang and T. E. Ferrin, *Structure* 2005, **13**, 473-482.

523 55 W. Kebsch and C.Sander, *Biopolymers* 1983, **22**, 2607-2673.

524 56 J. Dzubiella, *J. Am. Chem. Soc.* 2008, **130,** 14000-14007.

525 57 L. Triguero, R. Singh and R. Prabhakar, *J. Phys. Chem. B.* 2008, **112,** 7123-7131.

526 58 J. Zheng, H. Jang and R. Nussinov, *Biochemistry.* 2008, **47**, 2497

527 59 L. Shen, H. F. Ji and H. Y. Zhang, *J. Phys. Chem*. B. 2008, **112**, 3164.

528 60 N. D. Lazo, M. A. Grant, M. C. Condron, A. C. Rigby and D. B. Teplow, *Protein Sci.*

529 2005, **14**, 1611-1626.

530 61 J. M. Borreguero, B. Urbane, N. D. Lazo, S. V. Buldrev, D. B. Teplow and H. E. Stanley,

531 *Proc. Natl. Acad. Sci. U.S.A.* 2005, **102**, 6015-6020.

532 62 P. S. Hallman, D. D. Perrin and A. E. Watt, *Biochem. J.* 1971, **121**, 549-555.

533 63 D. Noy, I. Solomonov, O. Sinkevich, T. Arad, K. Kjaer, I. Saqi, *J. Am. Chem. Soc.*

534 2008,130, 1376-1383.

535

Graphical Abstract

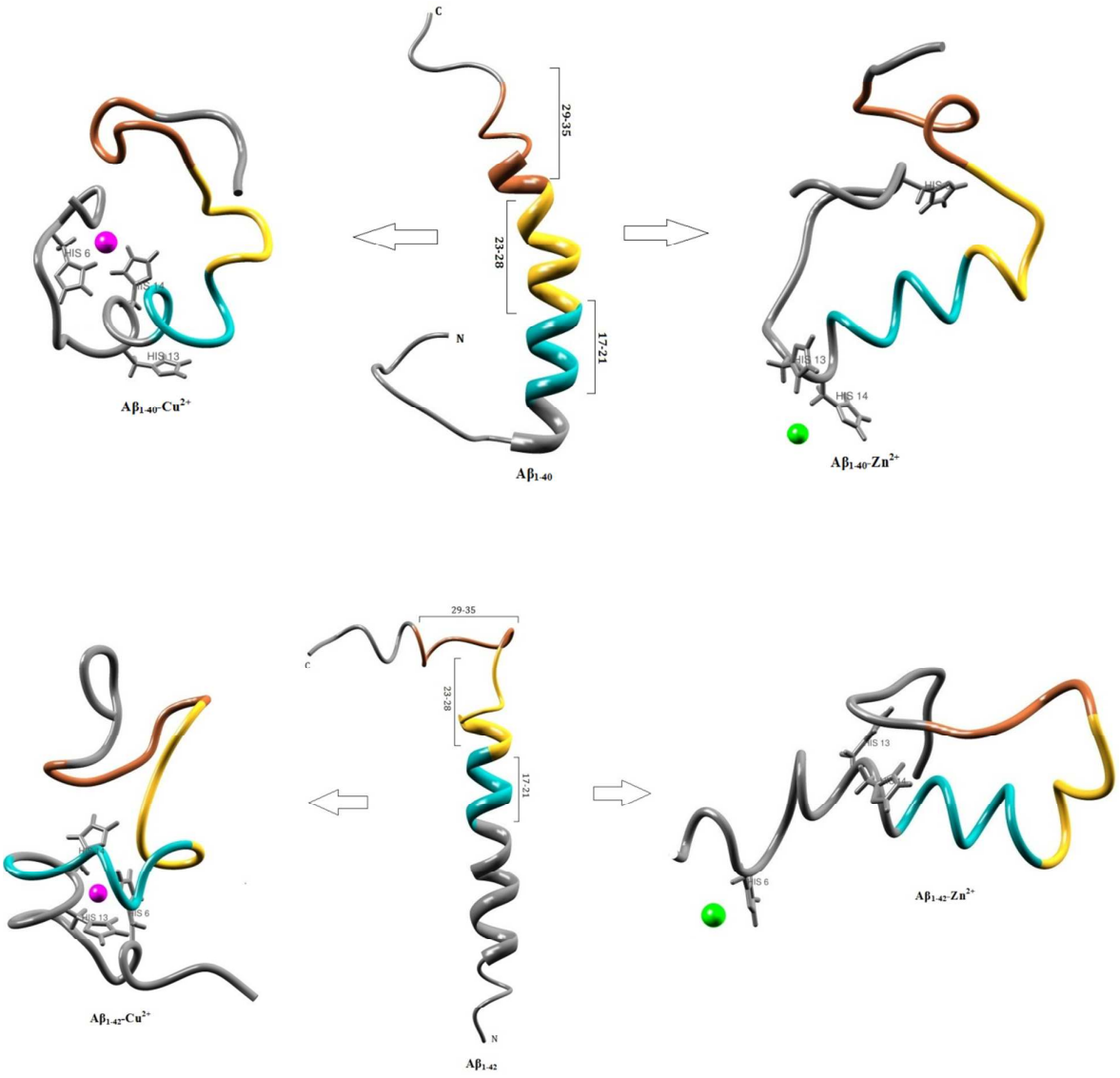

Conformational structural changes of $A\beta_{1-40}$ and $A\beta_{1-42}$ monomers during the interaction of Cu^{2+} and Zn^{2+} metal ions.

Fig. Caption

Fig. 1 RMSD plotted against time for all six structures**.**

Fig. 2 Secondary structural assignment per residue for the $A\beta_{1-40}$ monomer. (a) secondary structure as a function of time (b) Every 10ns interval of the $A\beta_{1-40}$ peptide were displayed and Cyan colour,17-21 residues; Golden rod colour, 23-28 residues; Sienna colour, 29-35 residues.

Fig. 3 Secondary structural assignment per residue for the $A\beta_{1-40}$-Cu^{2+}structure. (a) secondary structure as a function of time (b) Every 10ns interval of the $A\beta_{1-40}$ peptide were displayed and Cyan colour,17-21 residues; Golden rod colour, 23-28 residues; Sienna colour, 29-35 residues.

Fig. 4 Secondary structural assignment per residue for the $A\beta_{1-40}$-Cu^{2+}structure. (a) secondary structure as a function of time (b) Every 10ns interval of the $A\beta_{1-40}$ peptide were displayed and Cyan colour,17-21 residues; Golden rod colour, 23-28 residues; Sienna colour, 29-35 residues.
Fig. 5 Secondary structural assignment per residue for the $A\beta_{1-42}$ monomer. (a) secondary structure as a function of time (b) Every 10ns interval of the $A\beta_{1-42}$ peptide were displayed and Cyan colour,17-21 residues; Golden rod colour, 23-28 residues; Sienna colour, 29-35 residues.

Fig. 6 Secondary structural assignment per residue for the $A\beta_{1-42}$-Cu^{2+}structure. (a) secondary structure as a function of time (b) Every 10ns interval of the $A\beta_{1-42}$ peptide were displayed and Cyan colour,17-21 residues; Golden rod colour, 23-28 residues; Sienna colour, 29-35 residues.

Fig. 7 Secondary structural assignment per residue for the $A\beta_{1-42}$-Zn^{2+}structure. (a) secondary structure as a function of time (b) Every 10ns interval of the $A\beta_{1-42}$ peptide were displayed and Cyan colour,17-21 residues; Golden rod colour, 23-28 residues; Sienna colour, 29-35 residues.

Fig. 8 Contact map for (a) $A\beta_{1-40}$ (b) $A\beta_{1-40}$-Cu^{2+} (c) $A\beta_{1-40}$-Zn^{2+} (d) $A\beta_{1-42}$ (e) $A\beta_{1-42}$-Cu (f) $A\beta_{1-42}$-Zn^{2+} structures.

Fig. 9 SASA values Difference between (a) $A\beta_{1-40}$ and $A\beta_{1-42}$ monomer (b) $A\beta_{1-40}$-Cu^{2+} and $A\beta_{1-42}$- Cu^{2+} structure (c) $A\beta_{1-40}$-Zn^{2+} and $A\beta_{1-42}$-Zn^{2+} structure.

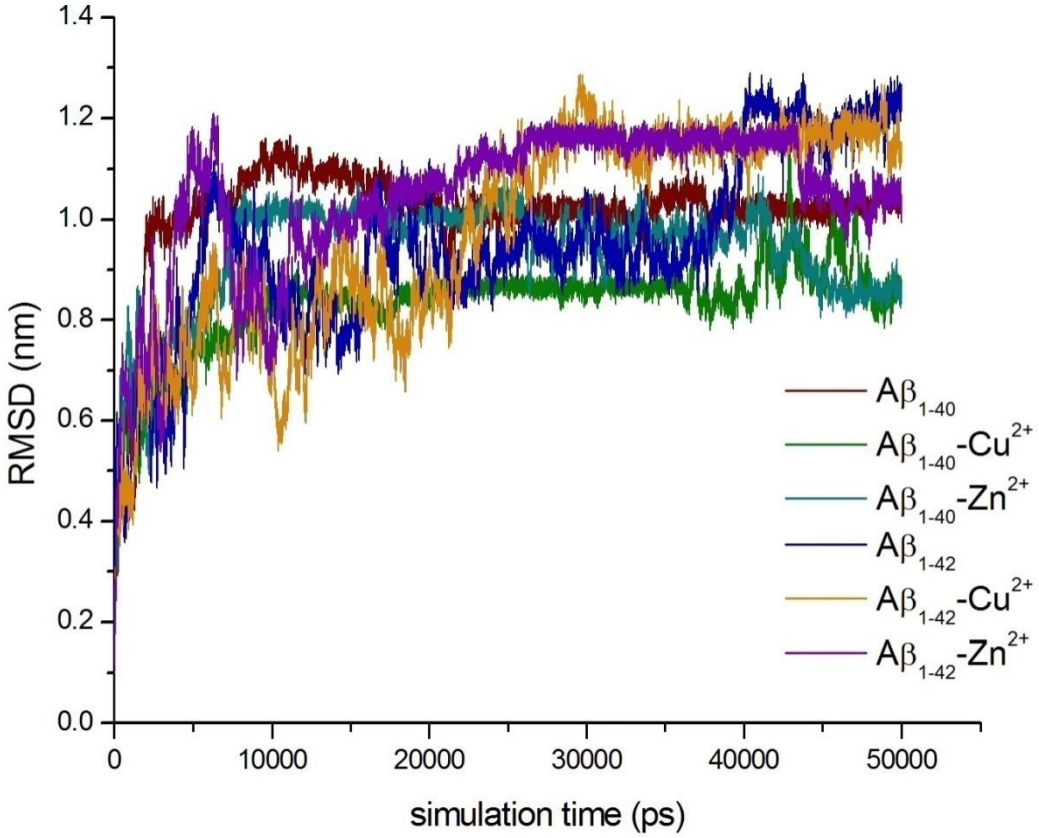

Fig. 1

a

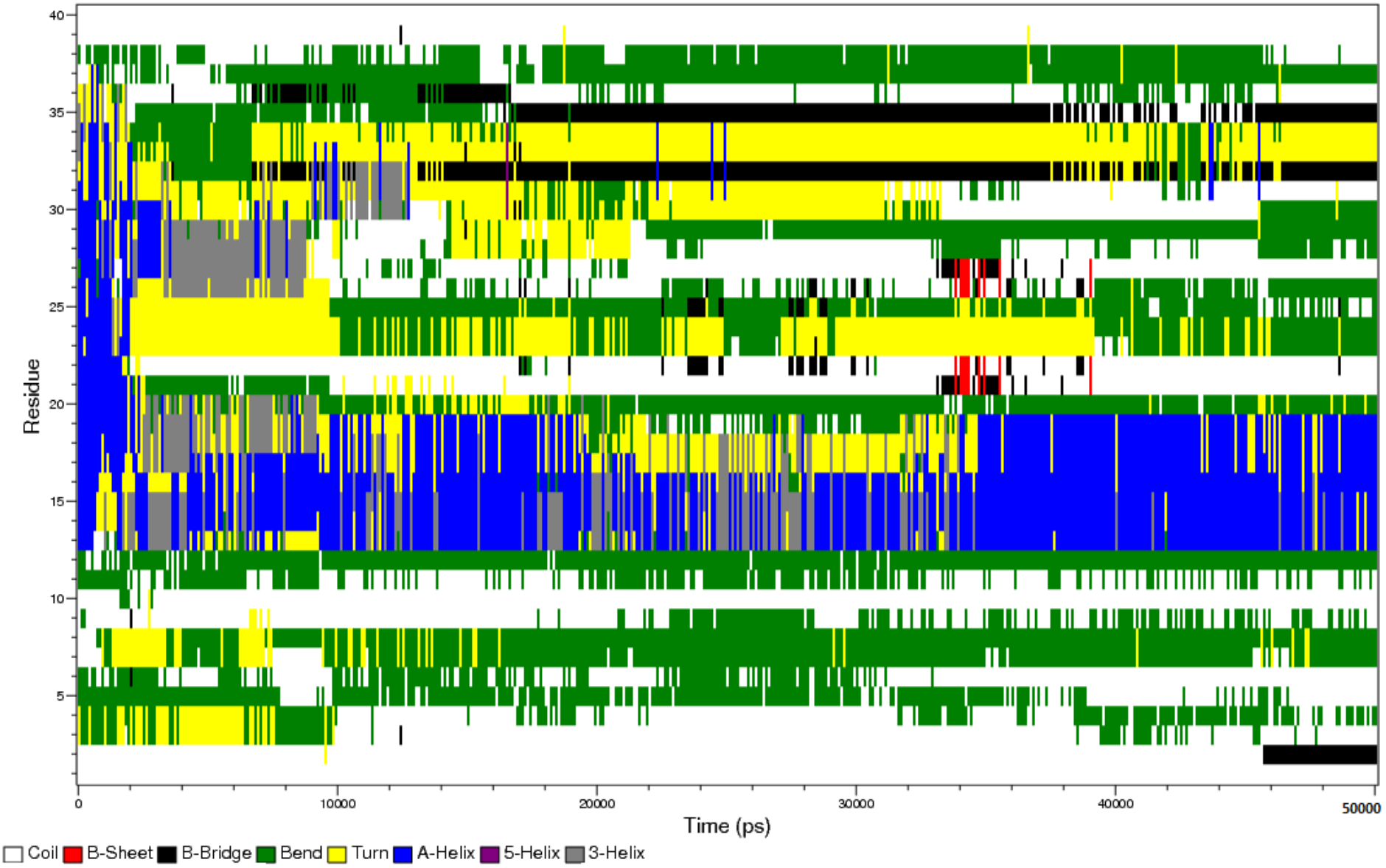

b

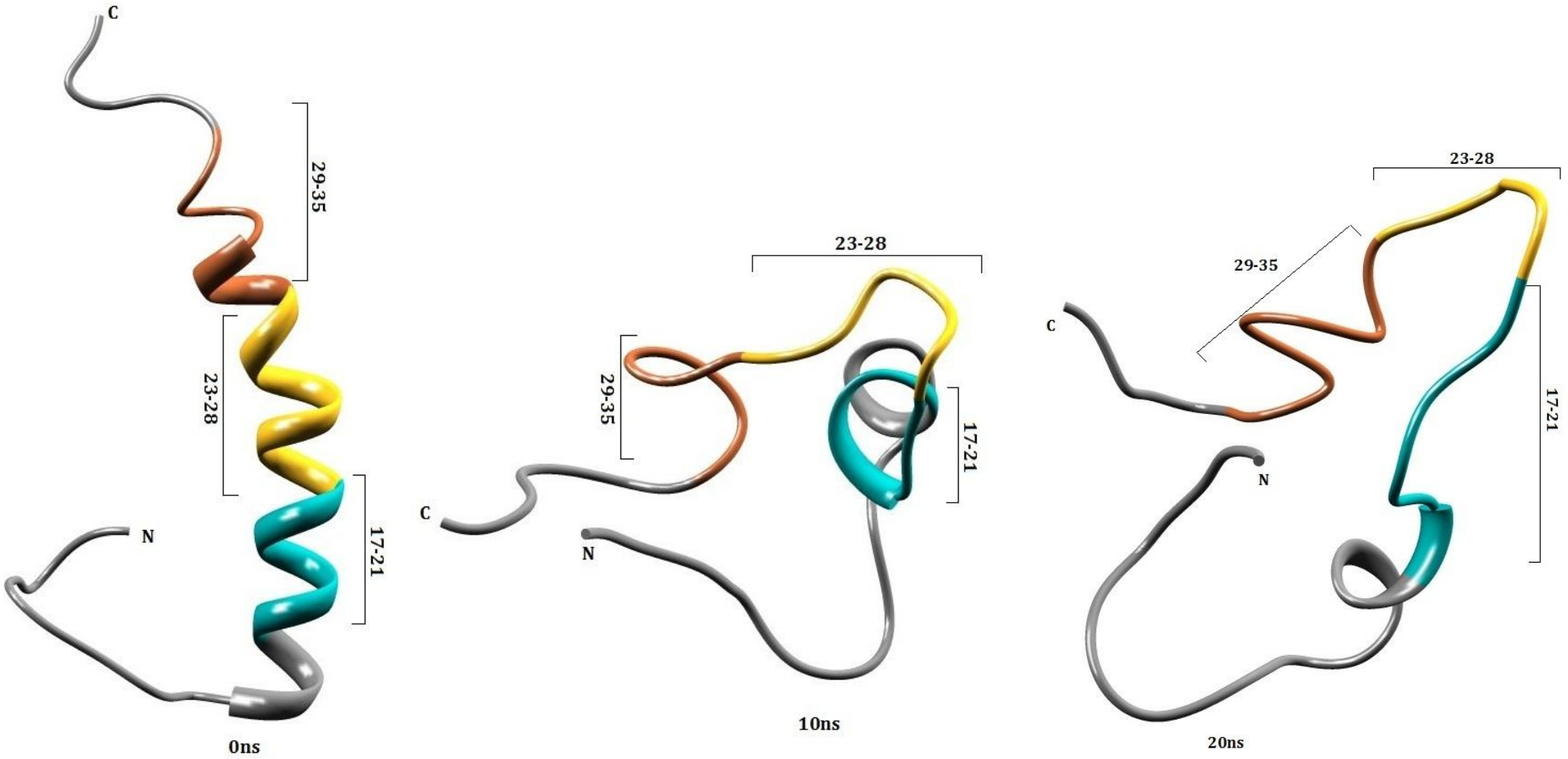

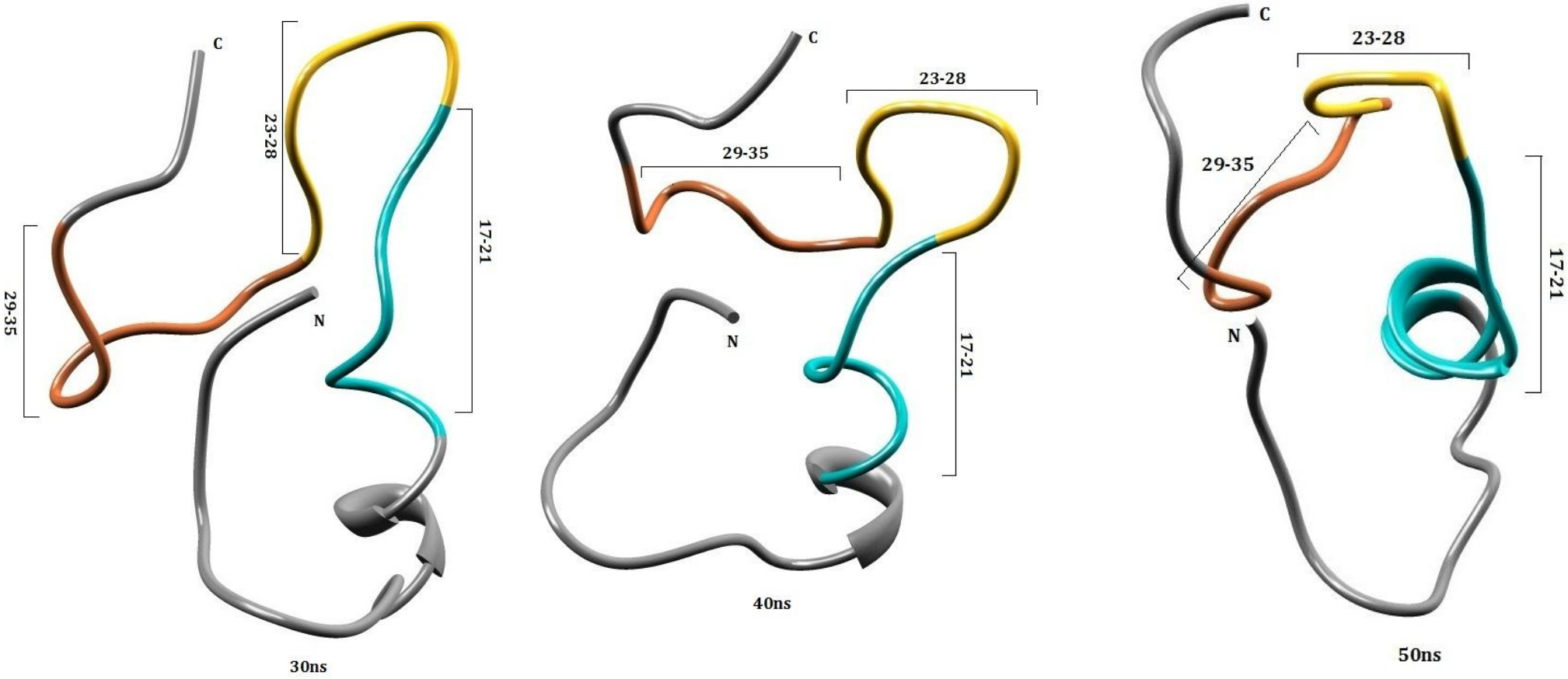

Fig. 2

a

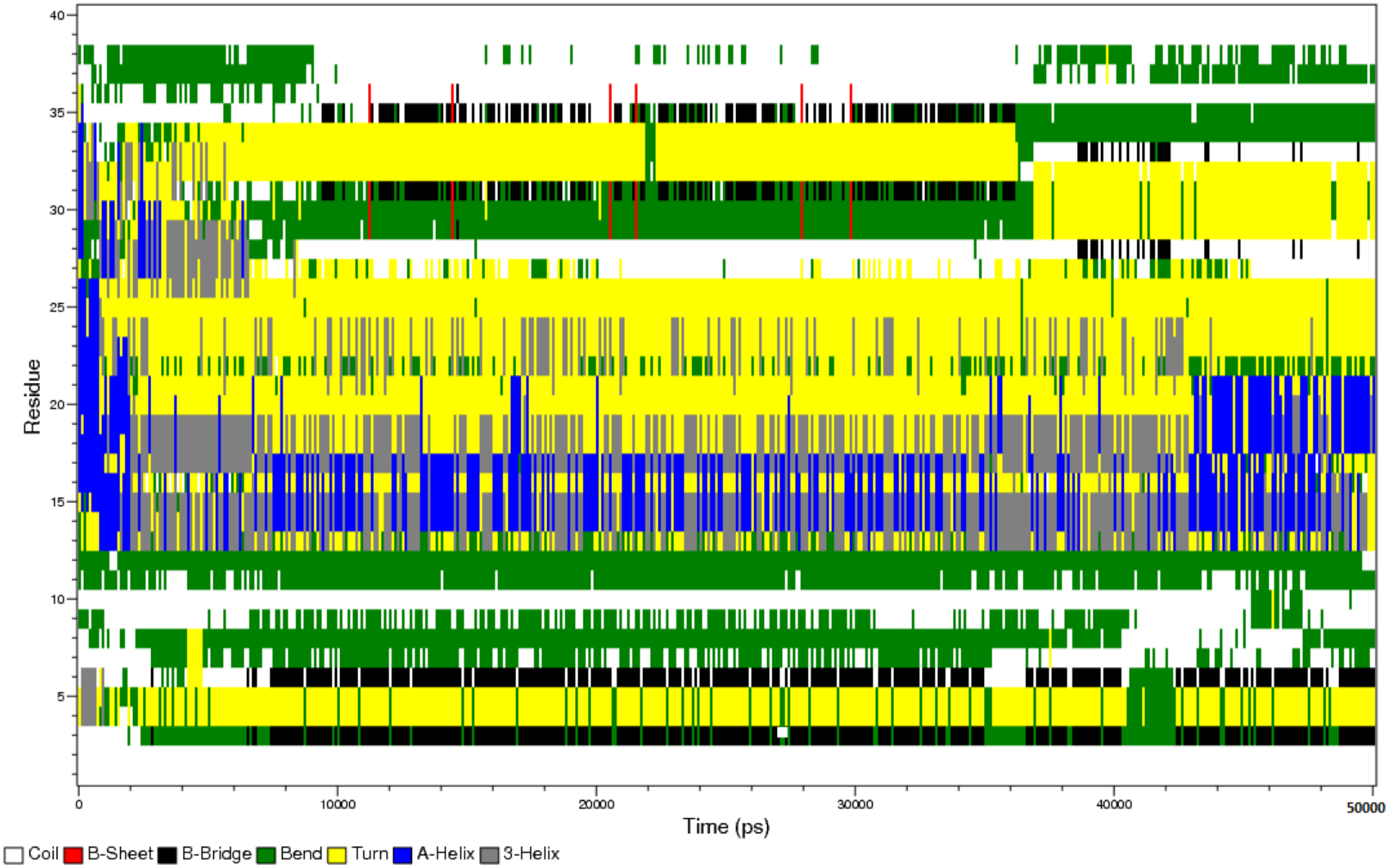

b

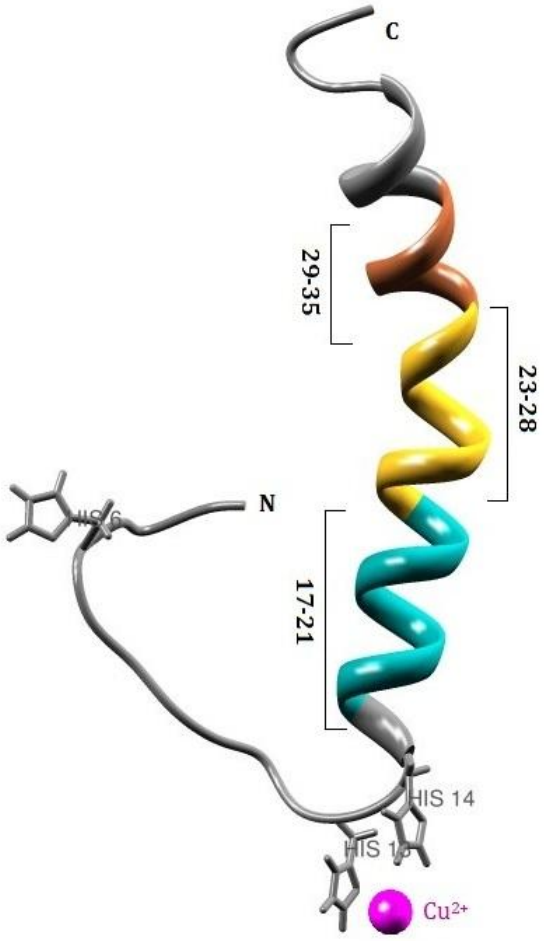

0ns

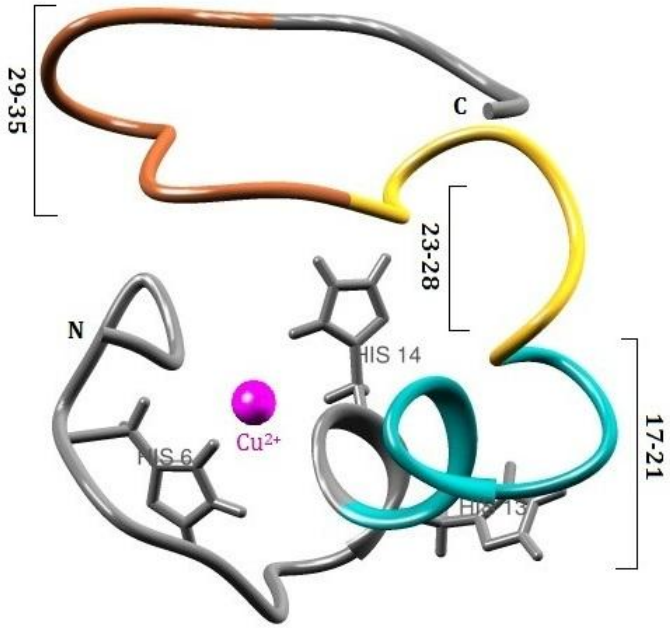

10ns

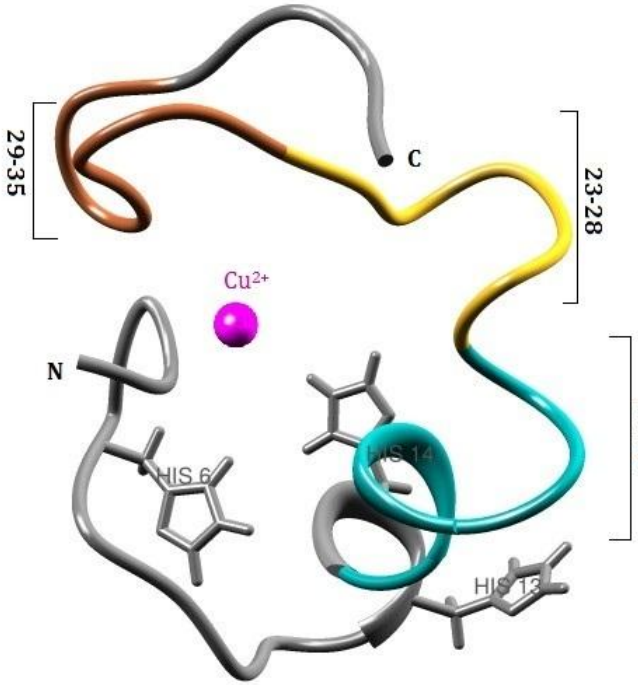

20ns

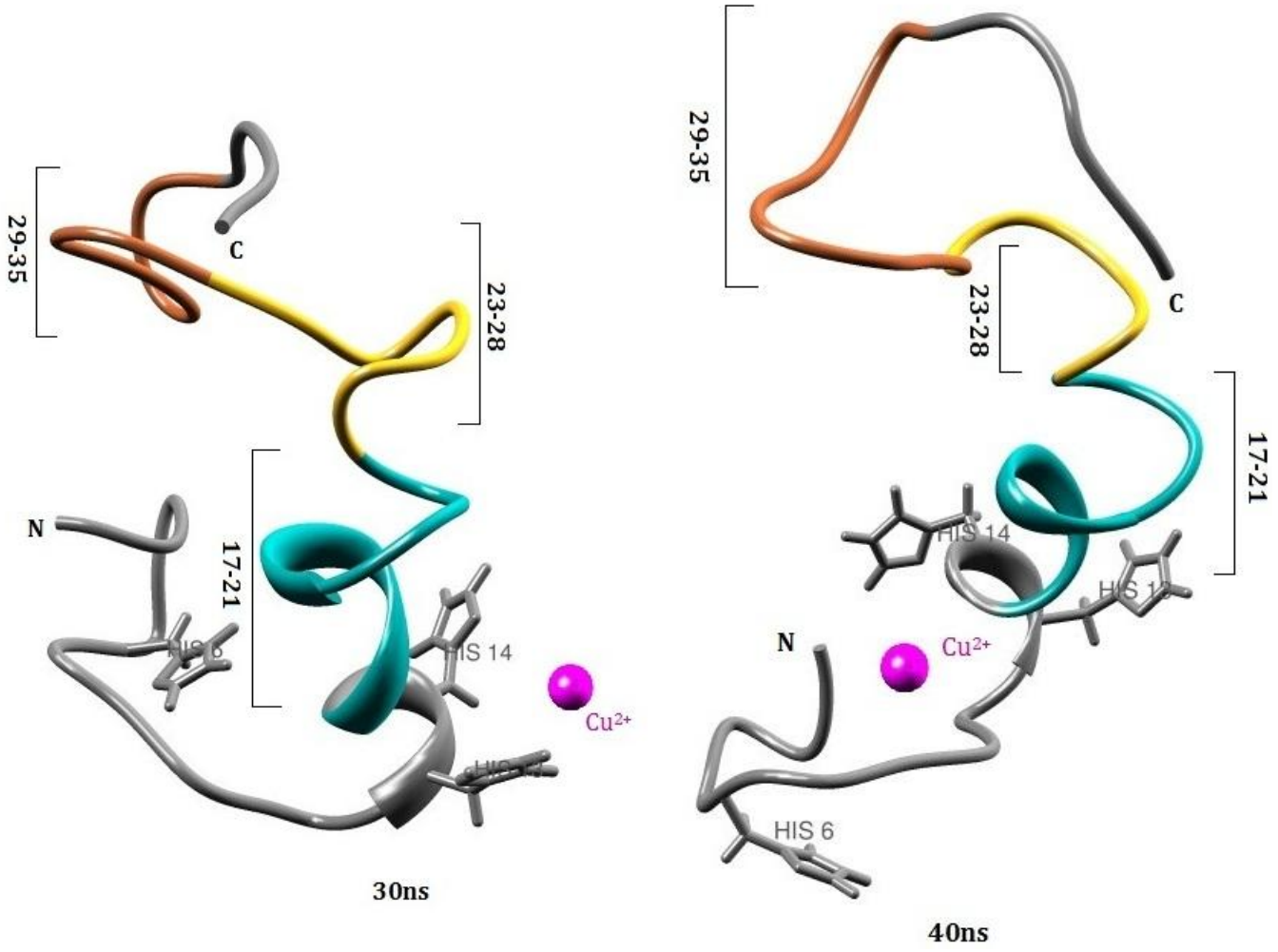

Fig. 3

a

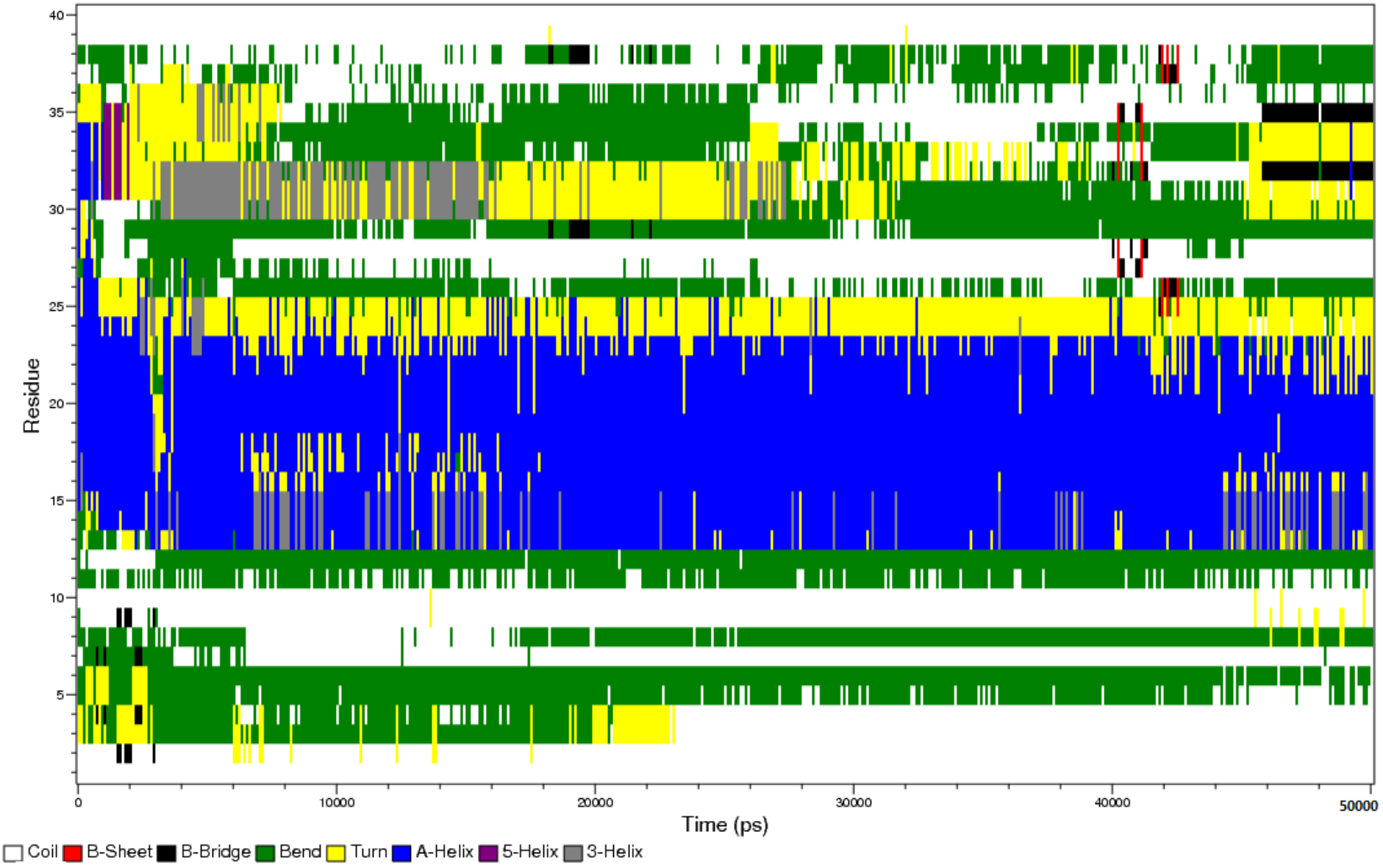

b

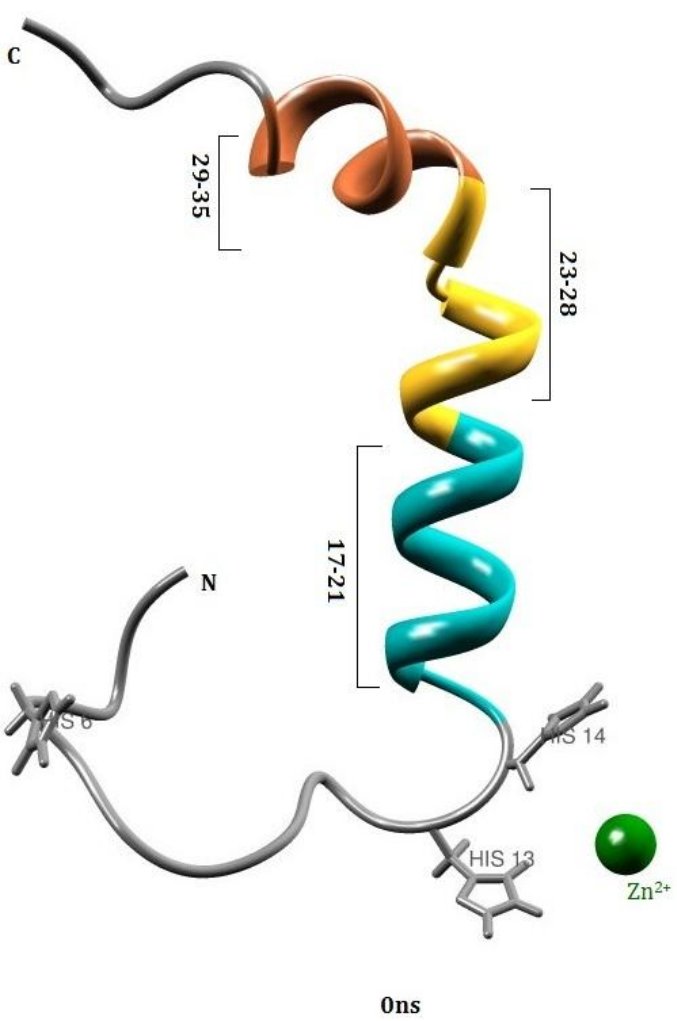

0ns

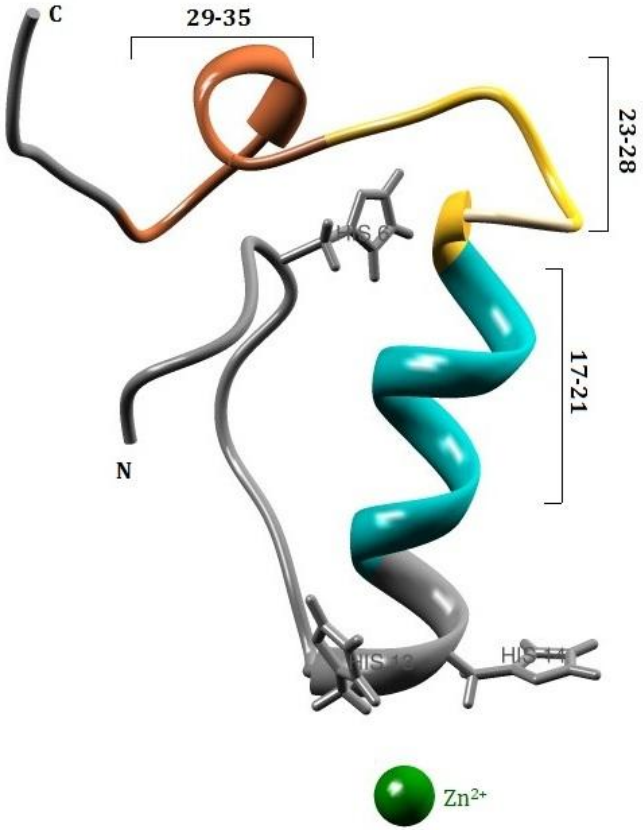

10ns

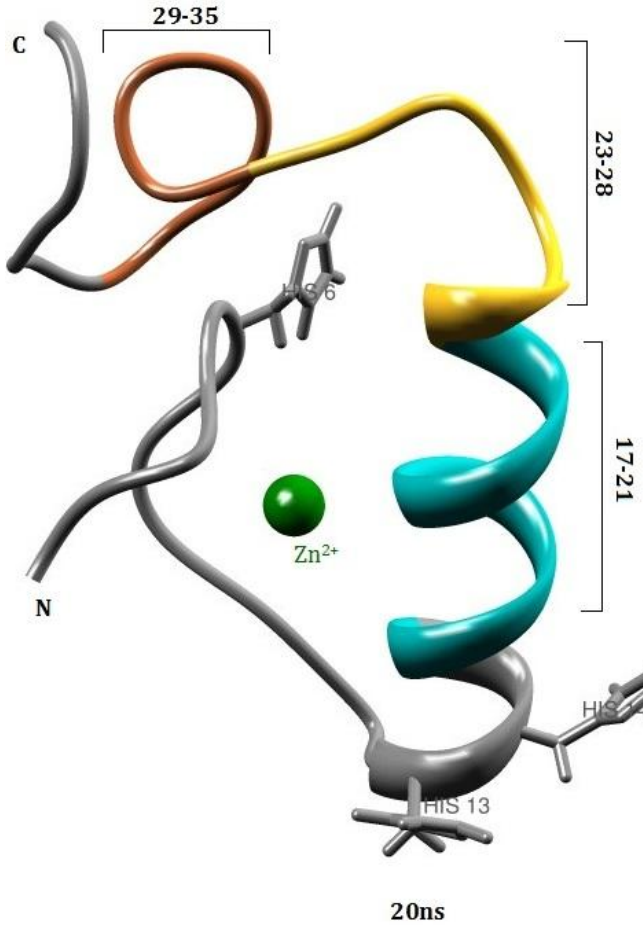

20ns

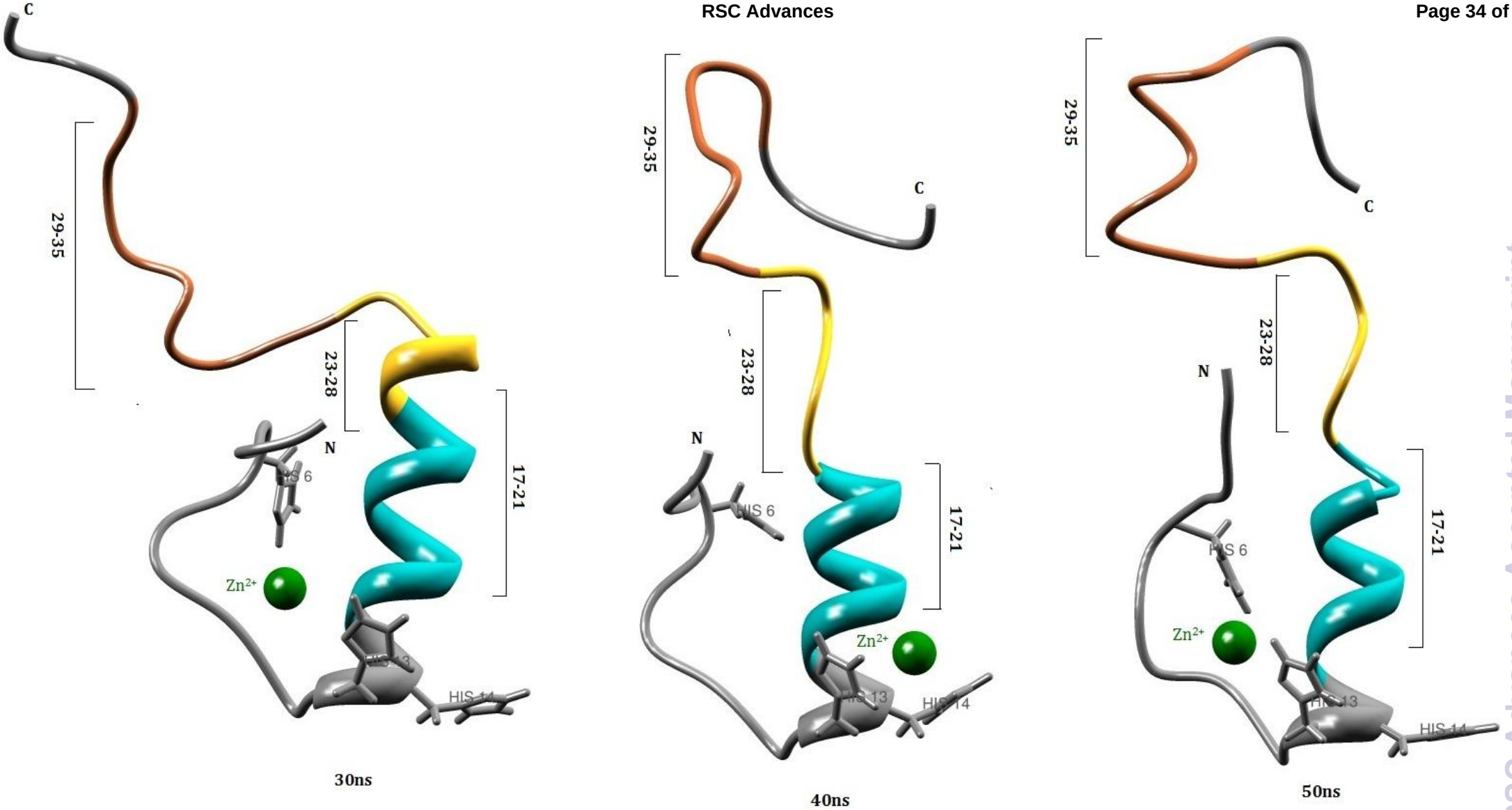

Fig. 4

a

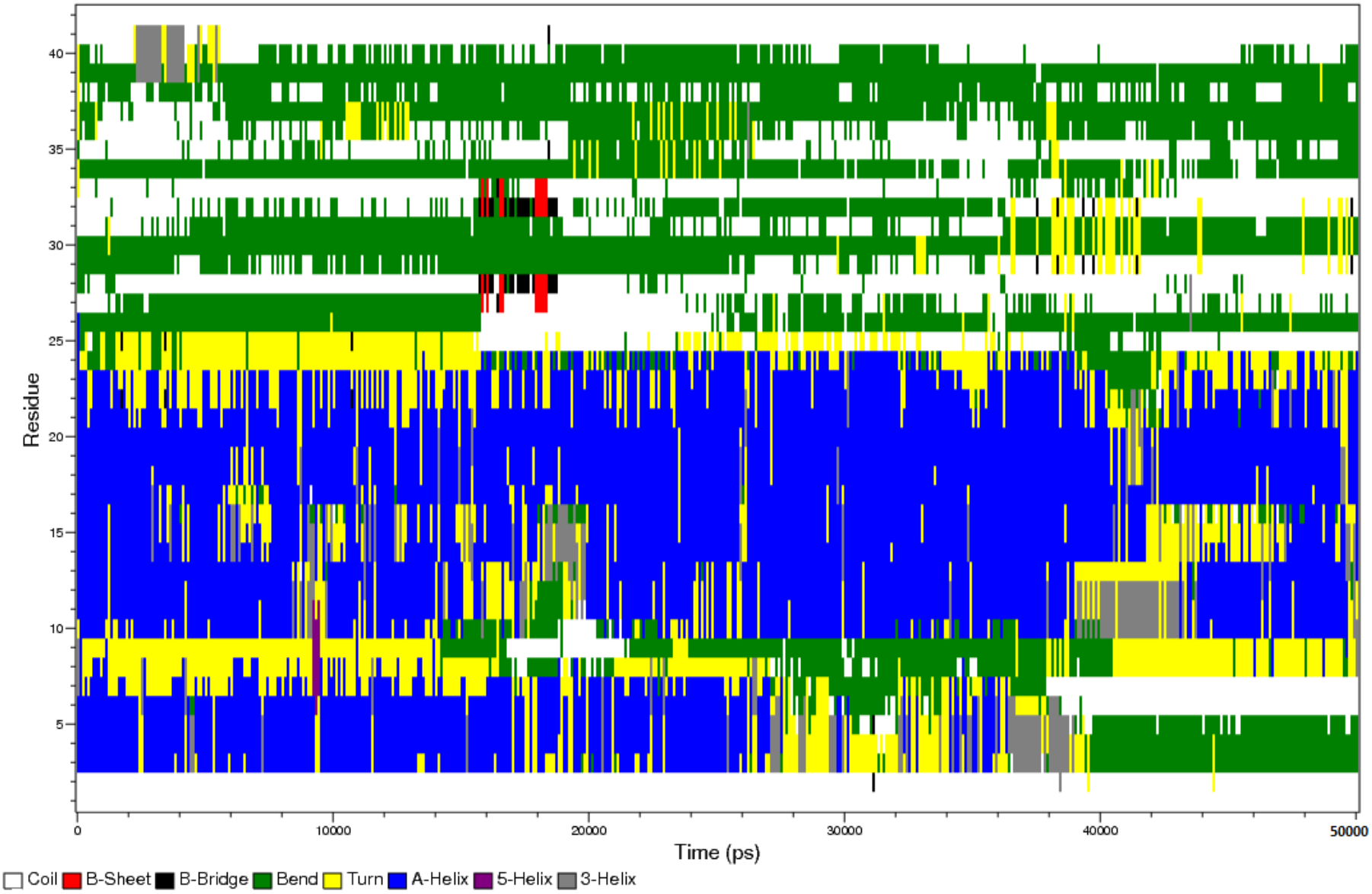

b

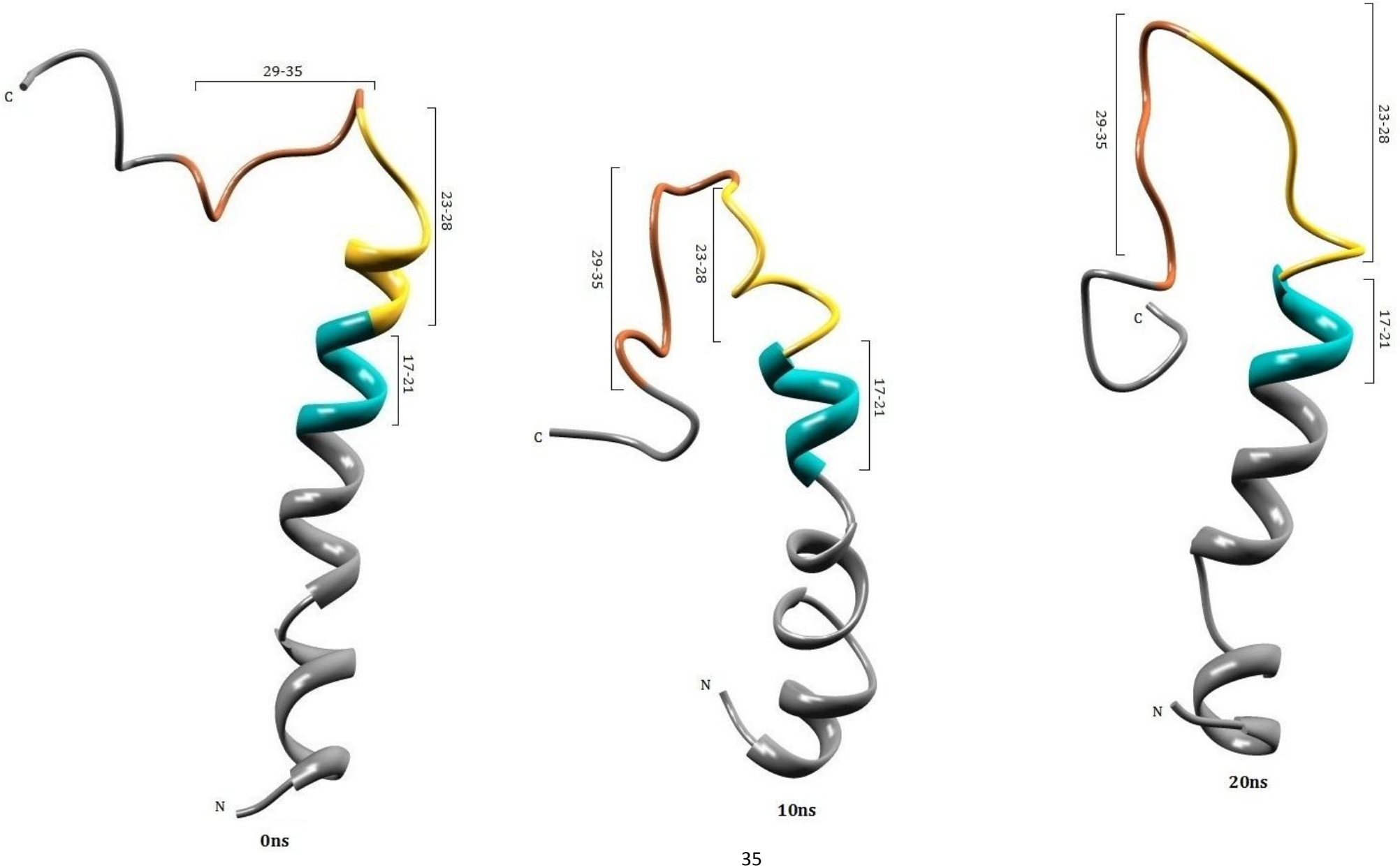

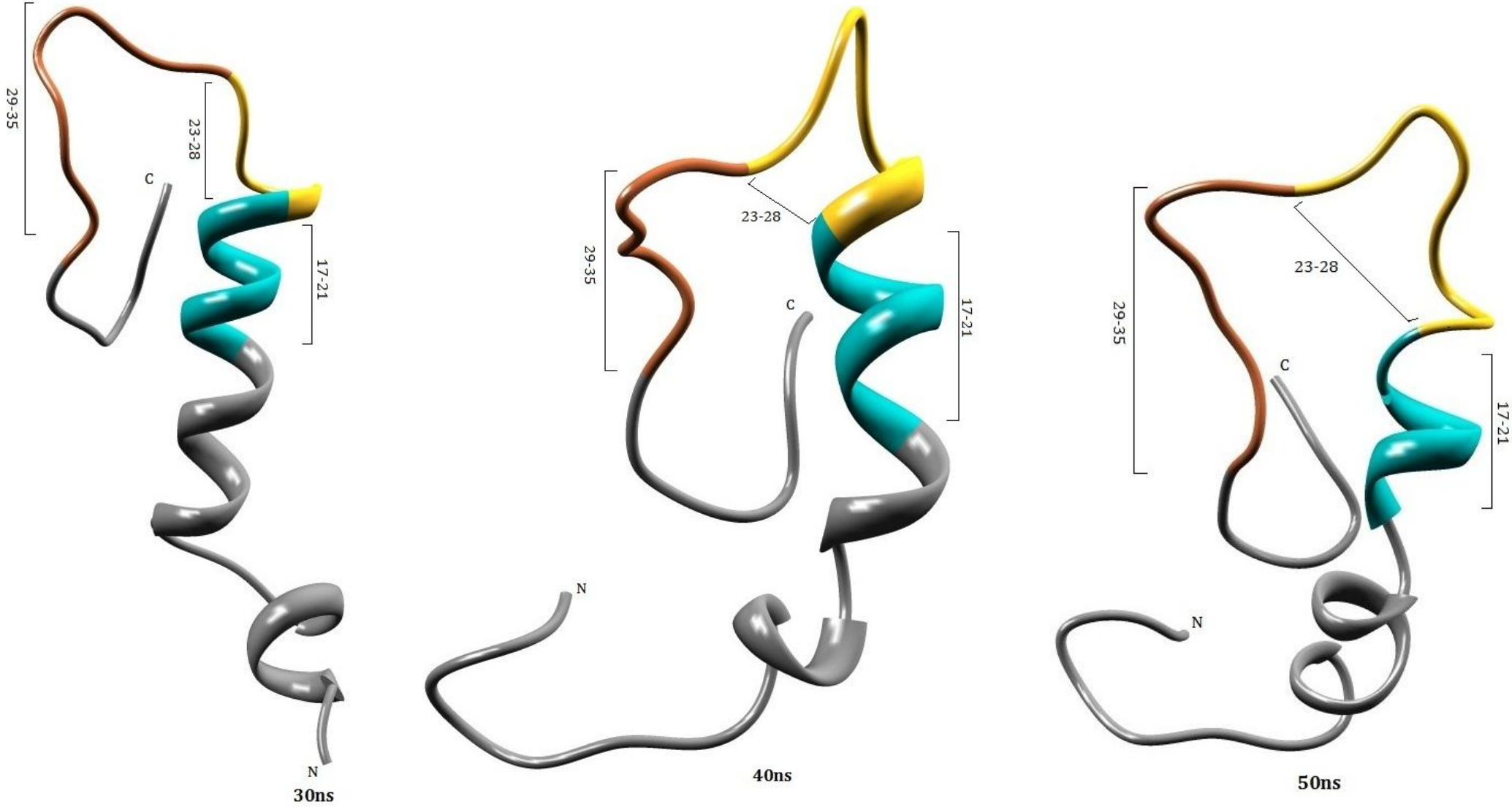

Fig. 5

a

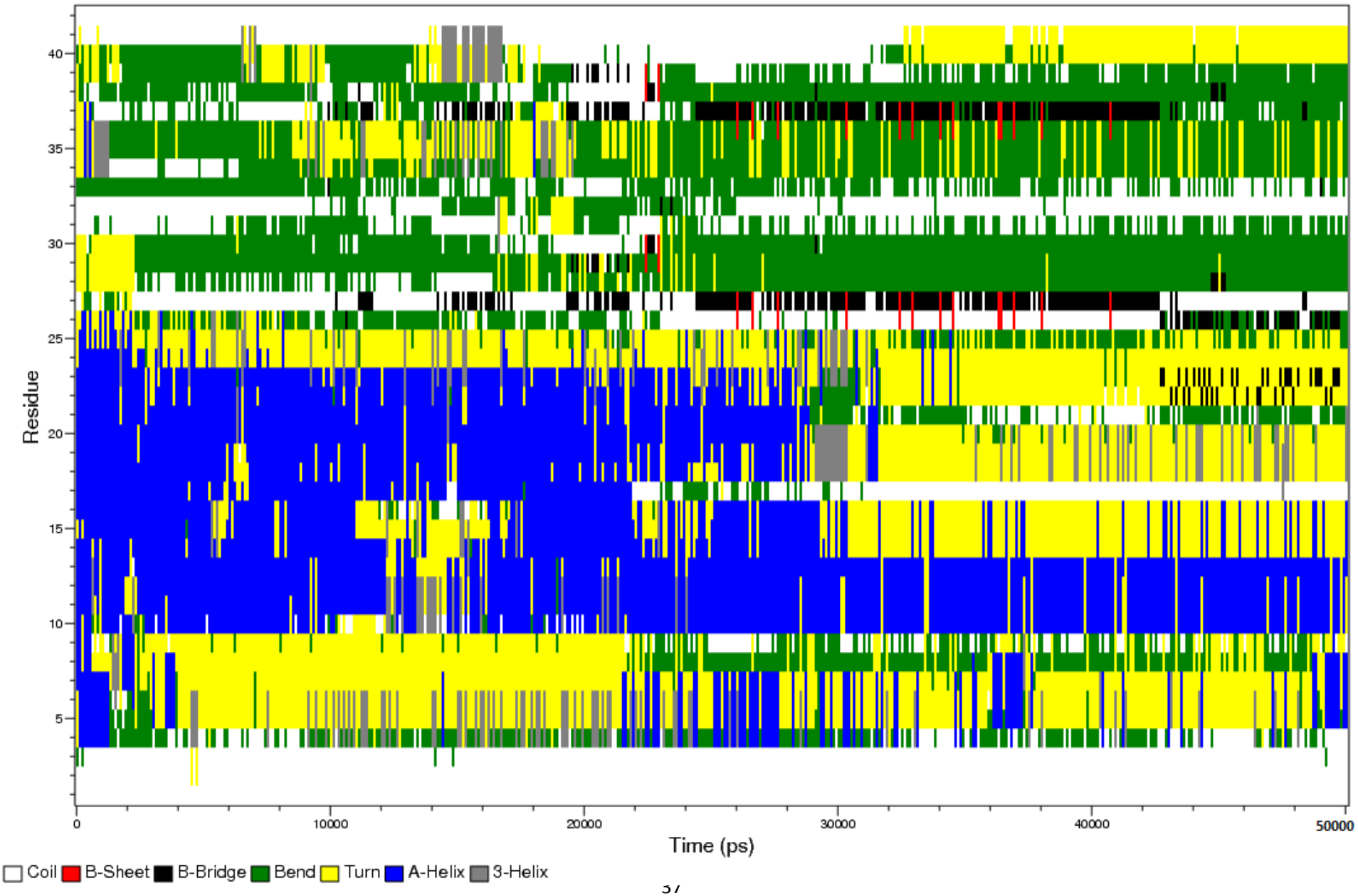

b

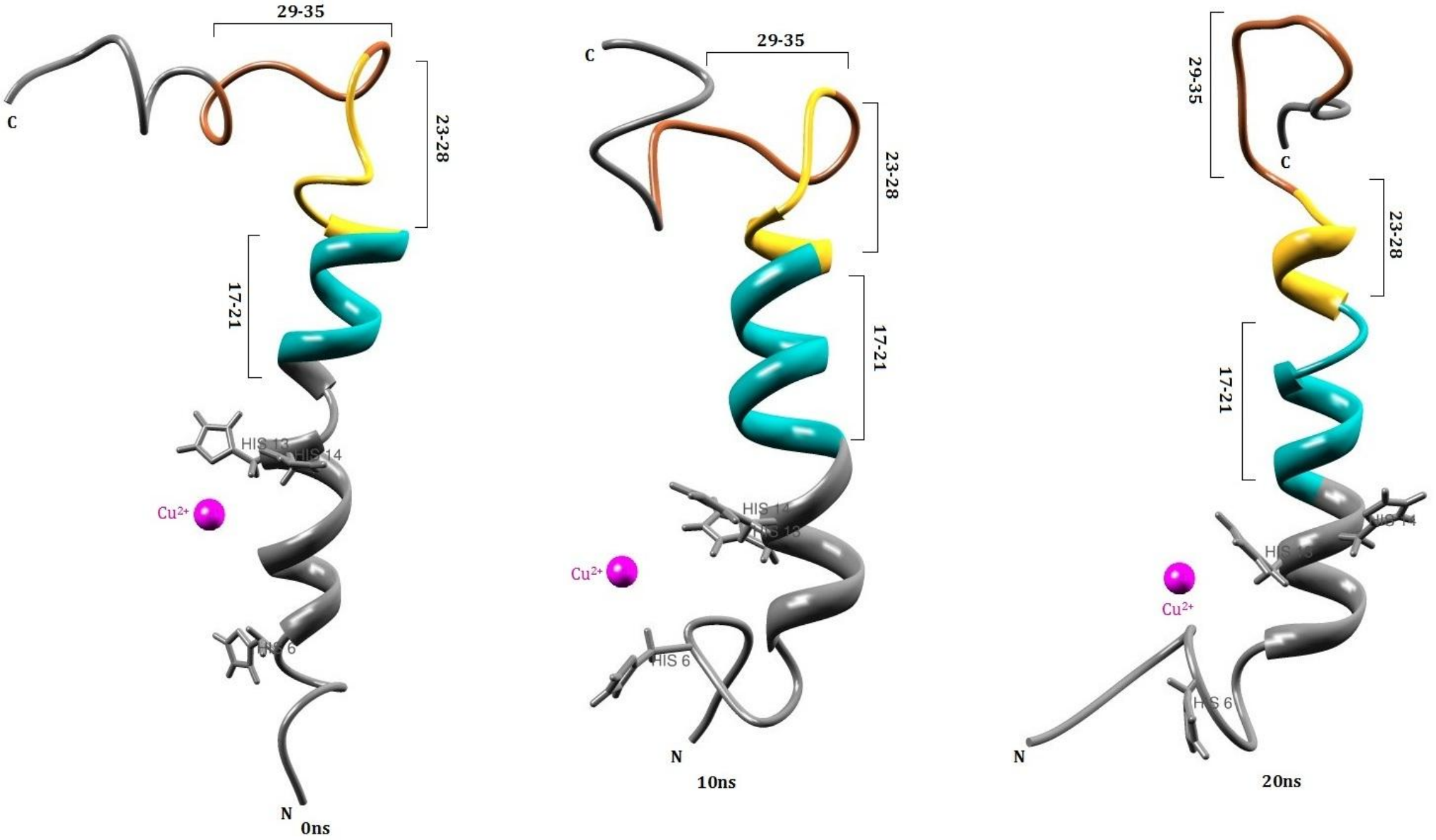

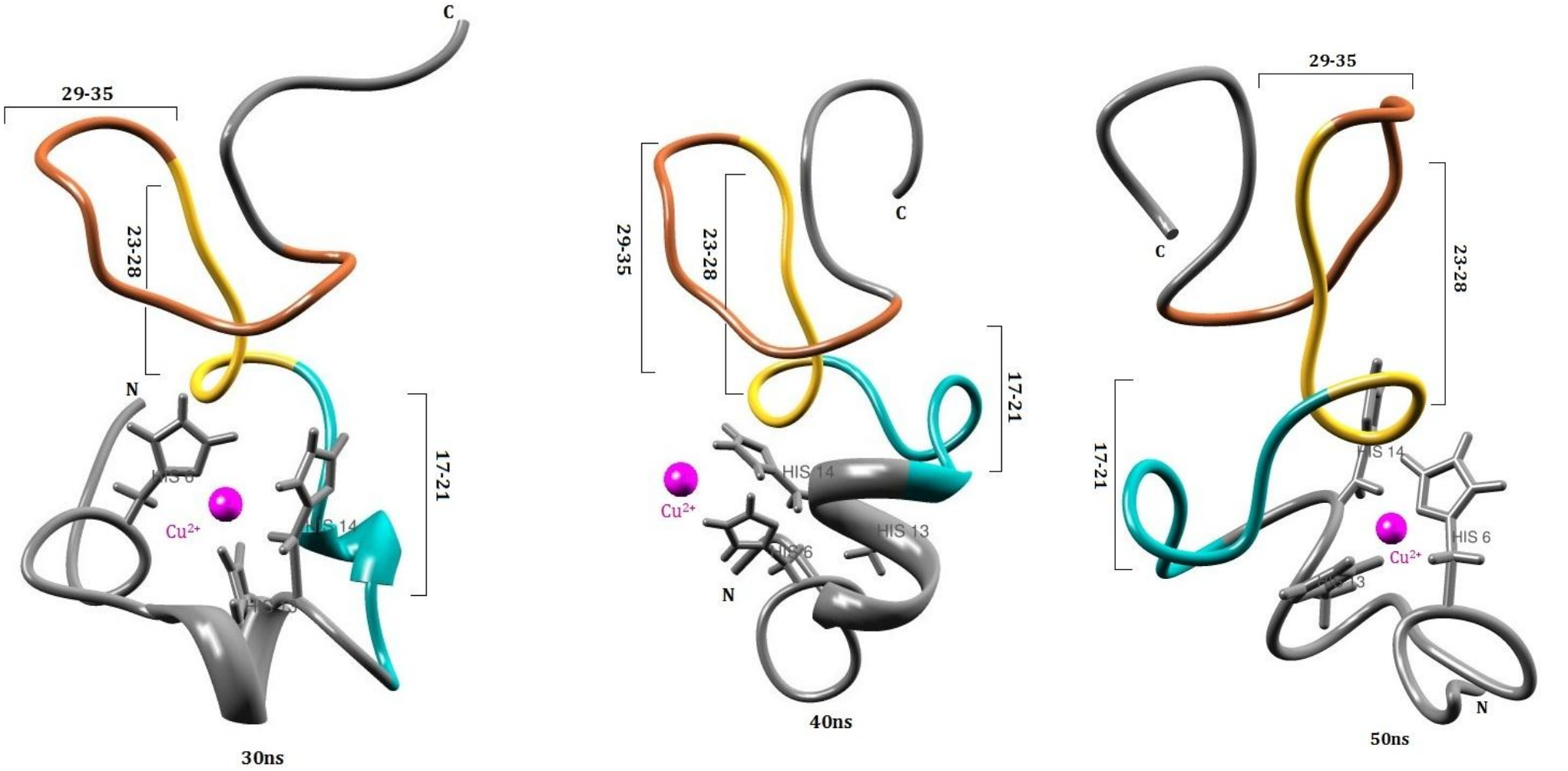

Fig. 6

a

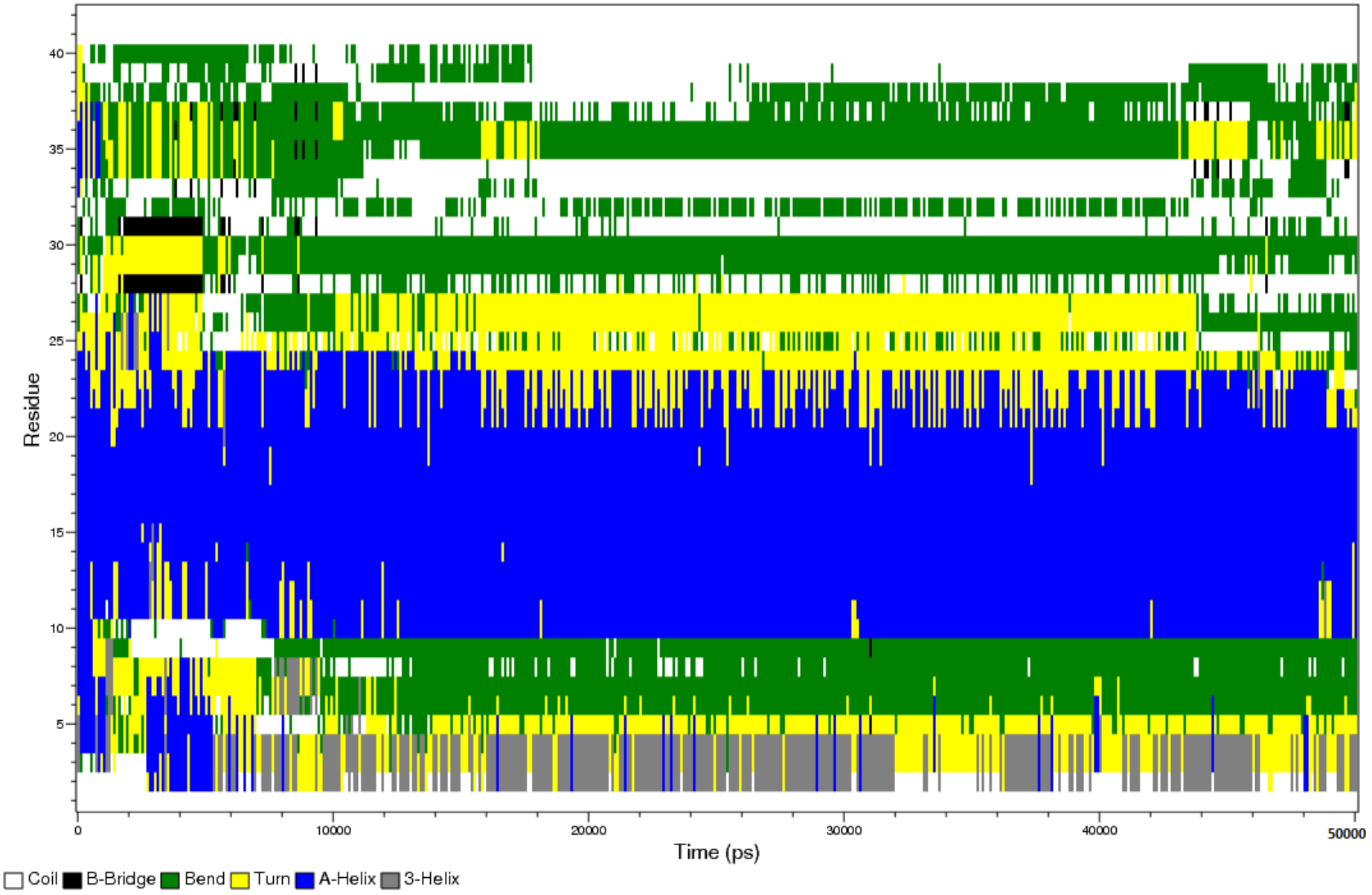

b

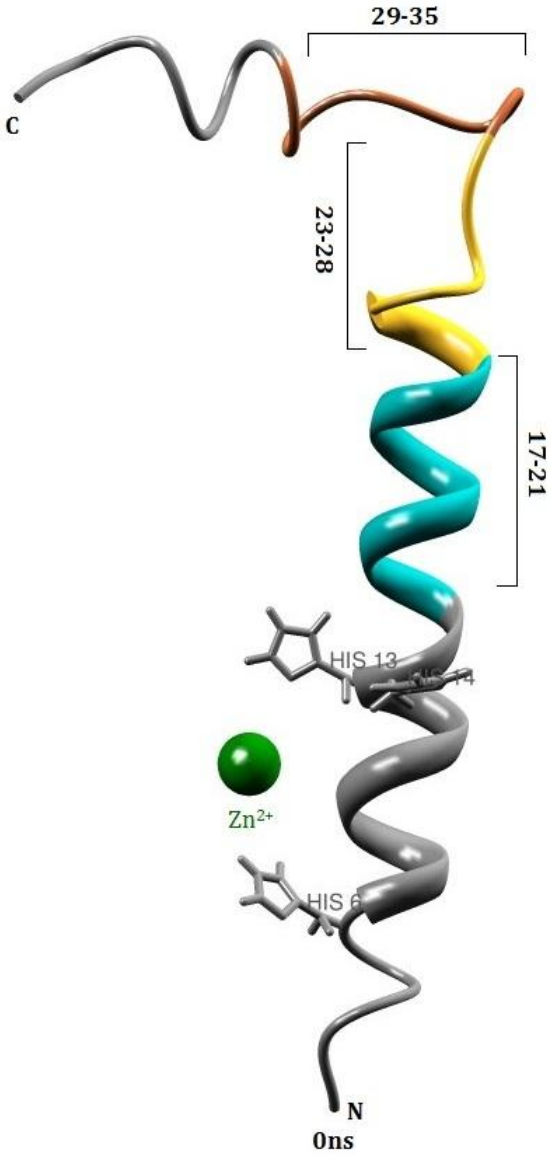

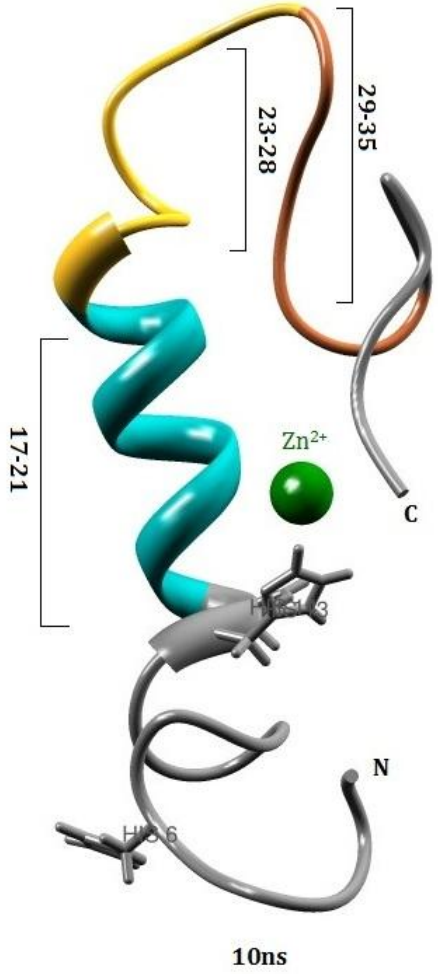

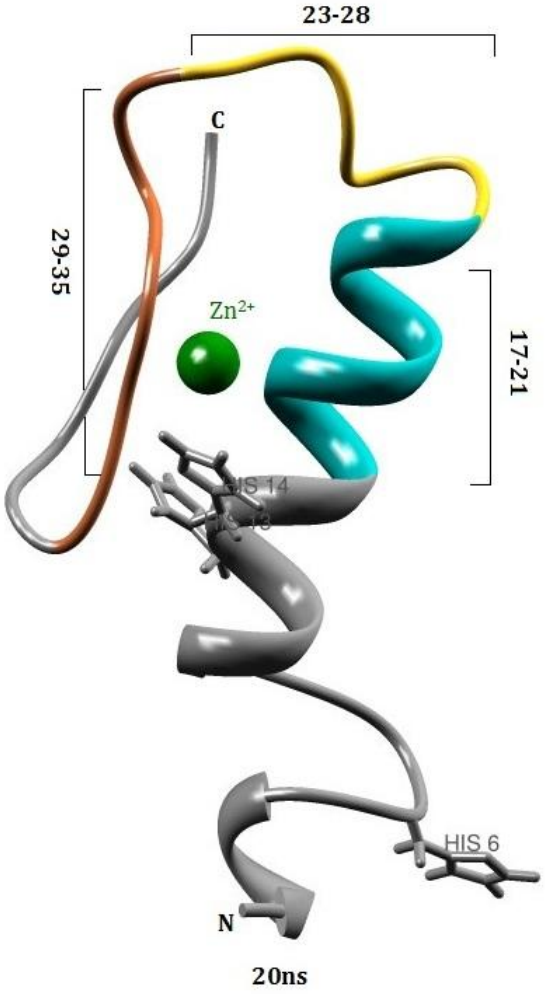

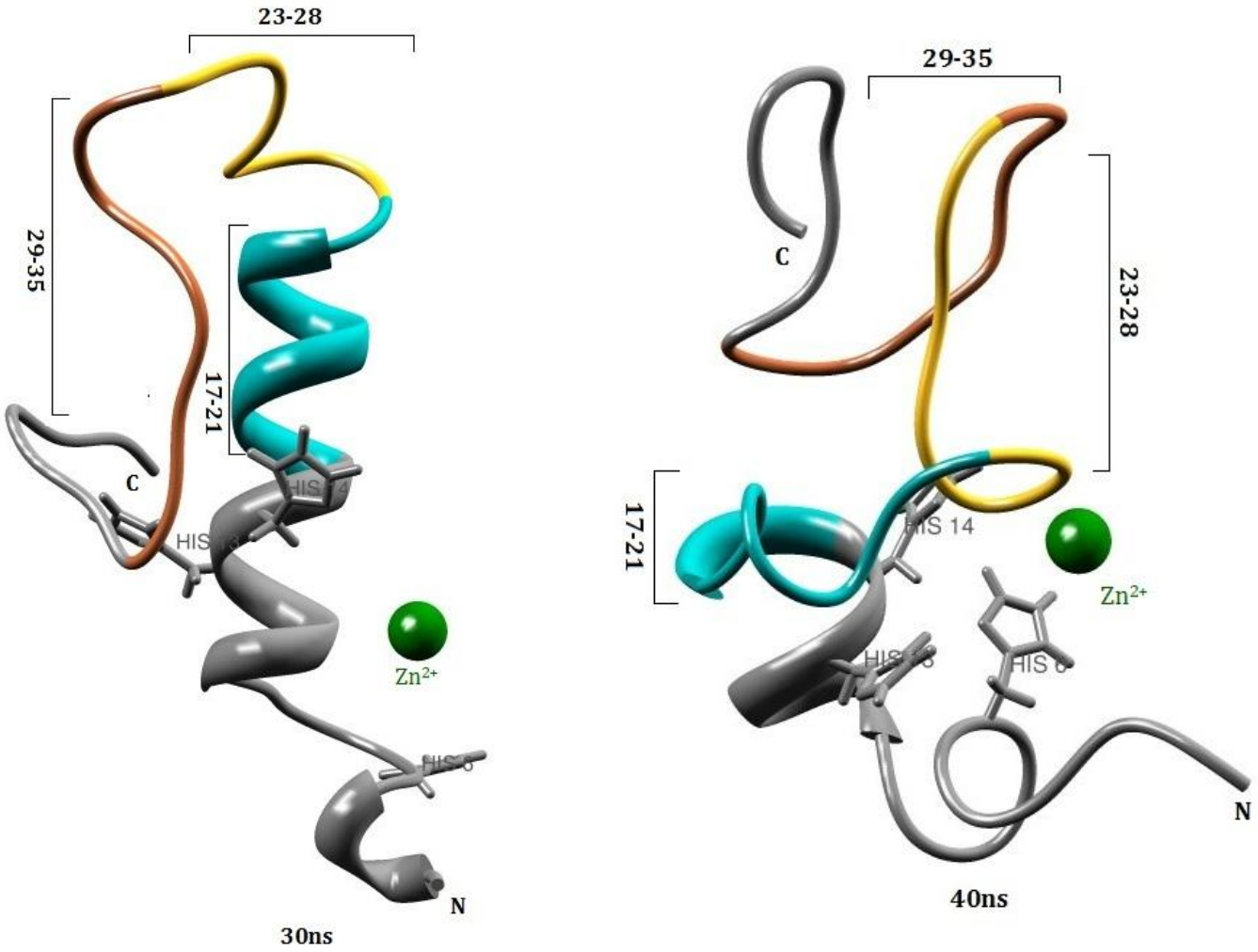

Fig. 7

a

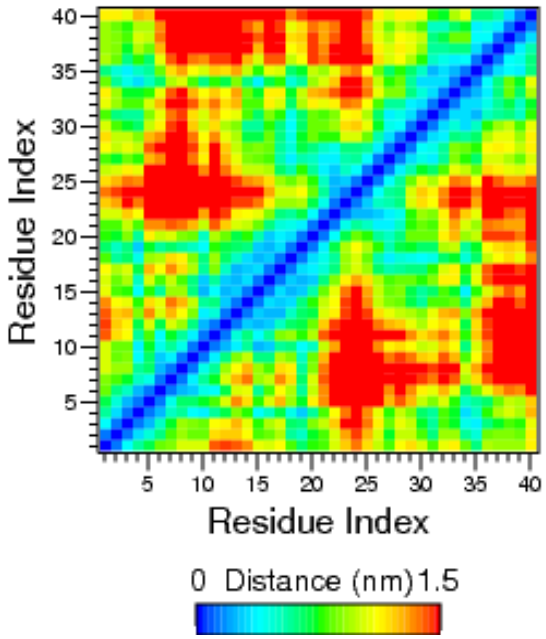

b

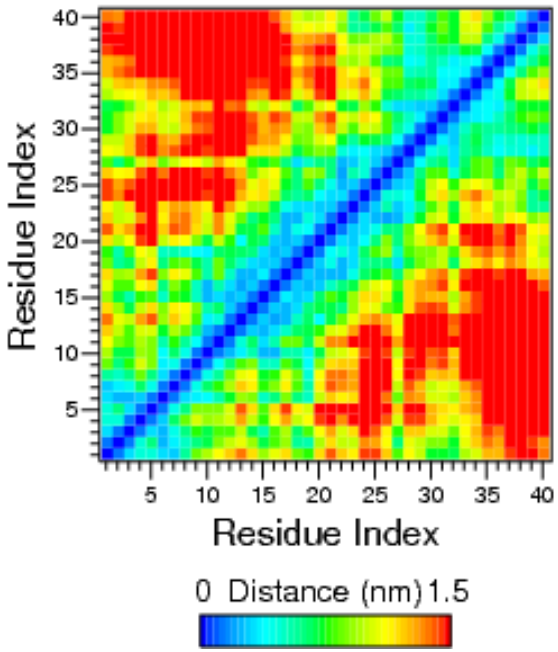

c

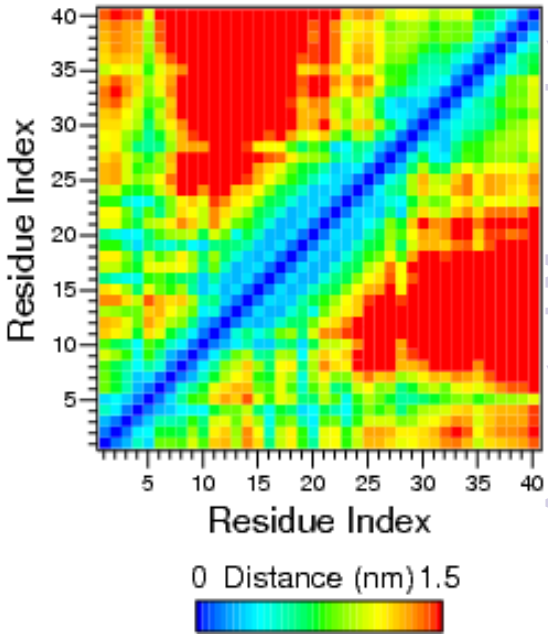

d e f

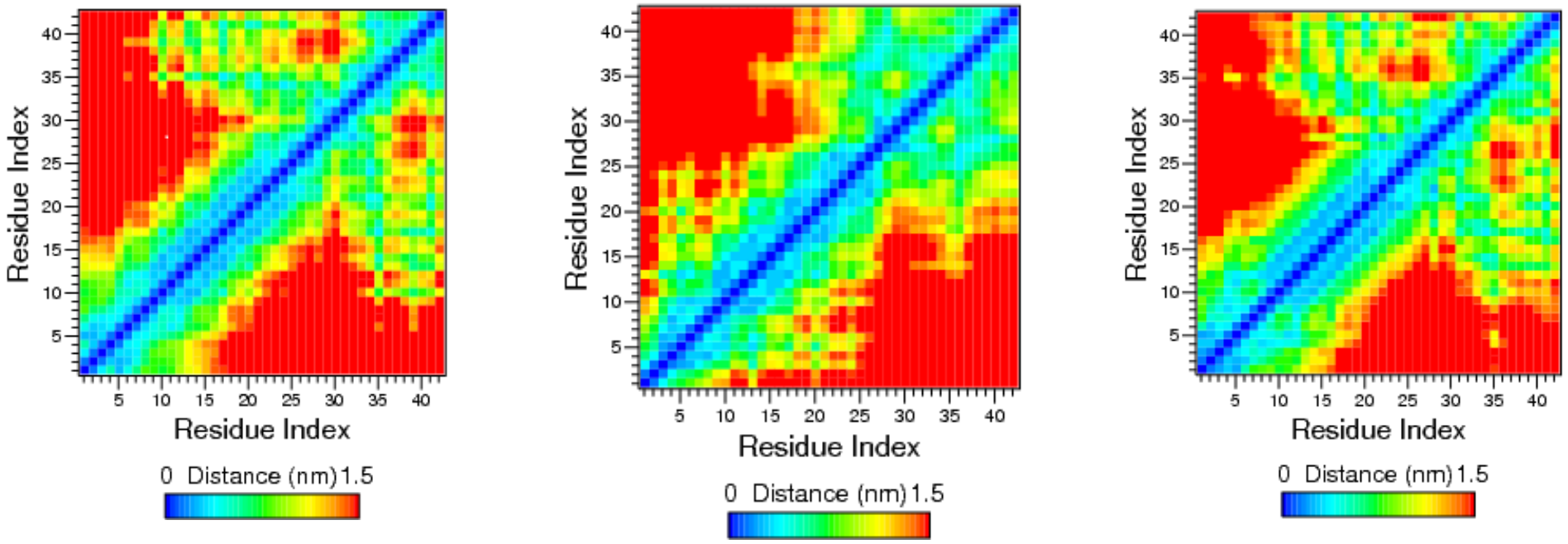

Fig. 8

a

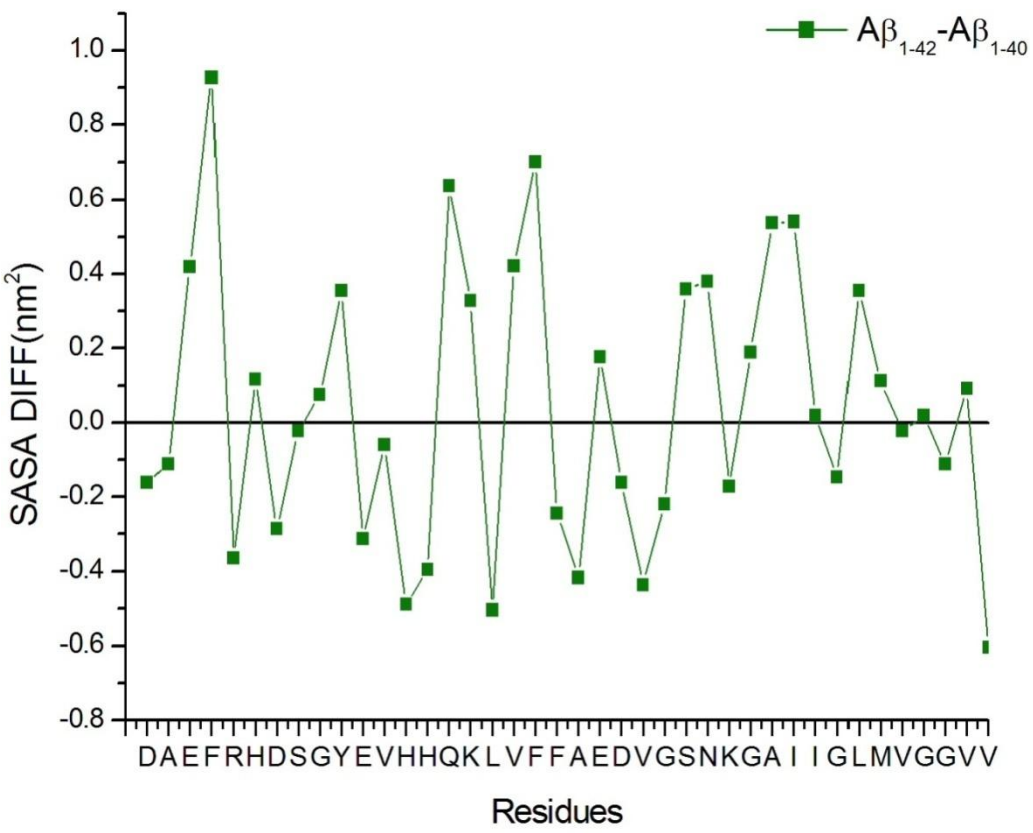

b

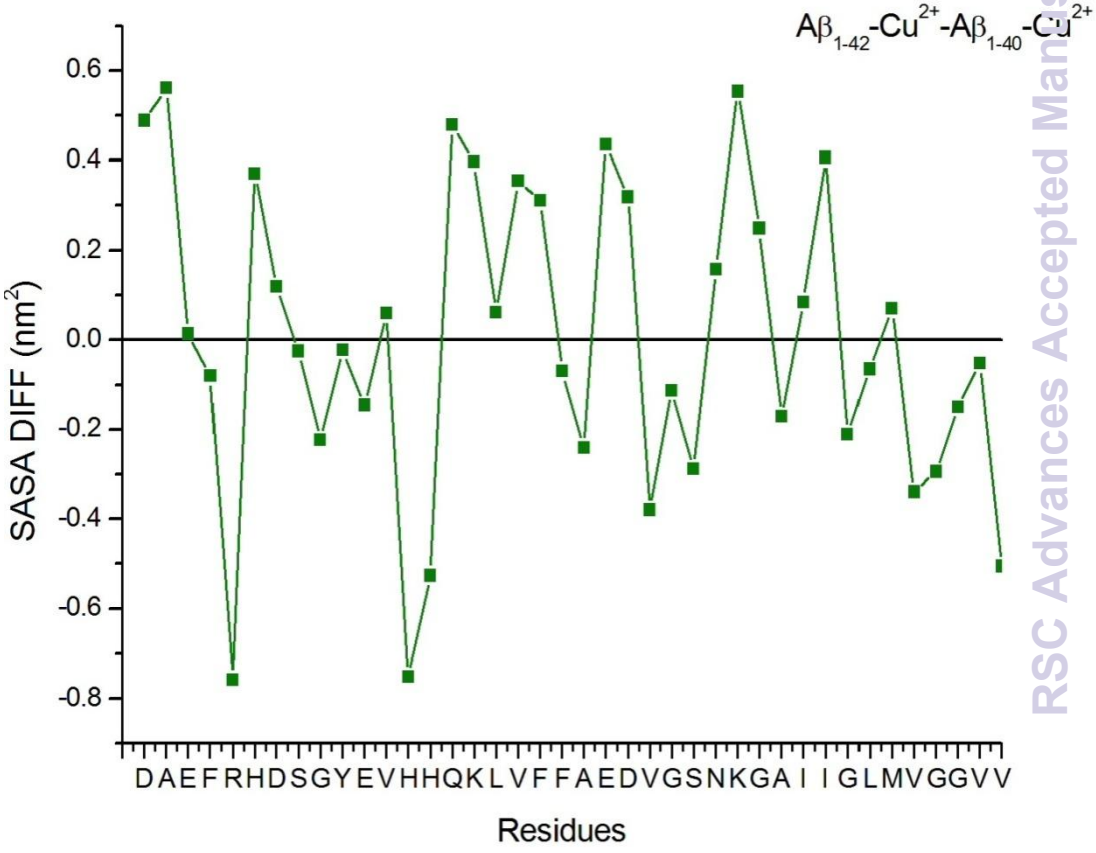

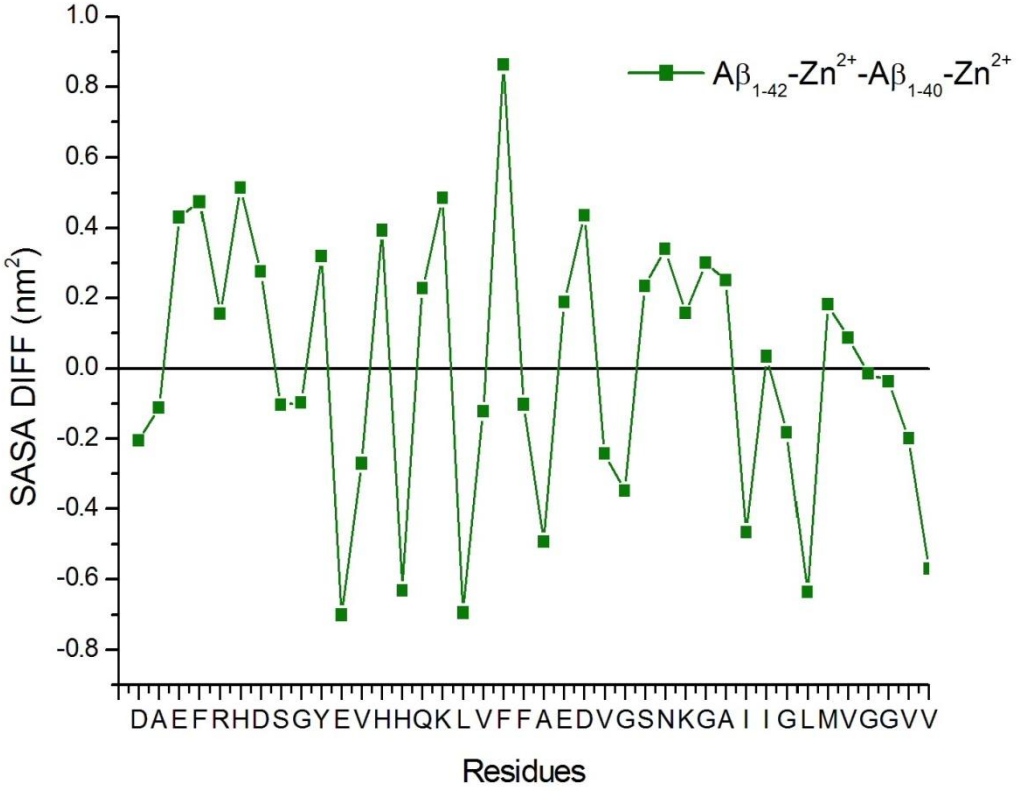

Fig. 9

Table 1 Percentage of Secondary structures calculated for $A\beta_{1-40}$, $A\beta_{1-40}$-Cu^{2+}, $A\beta_{1-42}$, $A\beta_{1-40}$-Zn^{2+}, $A\beta_{1-42}$-Cu^{2+}, and $A\beta_{1-42}$-Zn^{2+} structure in aqueous environment

	$A\beta_{1-40}$	$A\beta_{1-40}$-Cu^{2+}	$A\beta_{1-40}$-Zn^{2+}	$A\beta_{1-42}$	$A\beta_{1-42}$-Cu^{2+}	$A\beta_{1-42}$-Zn^{2+}
Coil	34	27	34	25	23	24
Beta	4	5	1	-	2	1
Bend	28	20	25	21	23	25
Turn	15	31	12	8	24	15
Helix	18	17	28	46	27	36